Available online at www.sciencedirect.com

ScienceDirect

Geochimica et Cosmochimica Acta 246 (2019) 41–59

Geochimica et Cosmochimica Acta

www.elsevier.com/locate/gca

Long-term monitoring of drip water and groundwater stable isotopic variability in the Yucatán Peninsula: Implications for recharge and speleothem rainfall reconstruction

Fernanda Lases-Hernandez [a,*], Martín Medina-Elizalde [b], Stephen Burns [c] Matthew DeCesare [b]

[a] Centro de Geociencias, UNAM Campus Juriquilla, Blvd. Juriquilla 3001, Posgrado en Ciencias de la Tierra, Juriquilla, Querétaro 76230, Mexico

[b] Department of Geosciences, Auburn University, 2050 Beard Eaves Memorial Coliseum, Auburn, AL 36849, United States

[c] Department of Geosciences, University of Massachusetts Amherst, 233 Morrill Science Center, Amherst, MA 01003, United States

Received 5 May 2018; accepted in revised form 15 November 2018; Available online 23 November 2018

Abstract

Hydroclimate interpretation of stalagmite $\delta^{18}O$ records from tropical regions requires an understanding of the temporal integration of rainfall amount and its isotopic composition by drip waters that form stalagmite deposits. This study presents oxygen ($\delta^{18}O$) and hydrogen (δD) isotopic results from over 1200 groundwater, rainfall and drip water samples, collected at ~weekly time intervals, over three hydrological years at Río Secreto Cave, in the Yucatán Peninsula, Mexico. Cave environmental conditions and the isotopic composition of drip water were monitored in three chambers with different degrees of air ventilation, along with temperature and relative humidity conditions at the surface. We examined 16 drips and observed that annual δD and $\delta^{18}O$ variability reflects the isotopic variability of rainfall to varying degrees. The observed annual amplitude of drip water isotopic variability represents between 5% and 95% of that of rainfall, reflecting epikarst water reservoir size and the complexity of flow paths. Drips that closely reflect the isotopic variability of rainfall and best preserve the isotopic signal of individual rainfall events are observed, but they are uncommon. Only two drips out of 16 were found to have potential to record rainfall isotopic shifts associated with tropical cyclones if sampled at weekly resolution. The relationship between δD and $\delta^{18}O$ in drip water suggests that recharge is biased toward the rainy season (June to November), which represents up to 80% of total annual precipitation. We find that over the course of a year most drips reflect the annual $\delta^{18}O$ composition of rainfall, in support of quantitative precipitation estimates from stalagmite $\delta^{18}O$ records. We find evidence that the effective recharge in this cave system is controlled by precipitation amount and that recharge is not limited to the months when precipitation exceeds evaporation.

Keywords: $\delta^{18}O$; δD; Speleothem; Tropical cyclones; Vadose hydrology; Effective recharge; Cave

1. INTRODUCTION

Paleoclimate studies provide an essential tool to predict future climate change and to assess the extent to which human and biological adaptation is realistic under business-as-usual scenarios of anthropogenic greenhouse gas emissions. Recent efforts, in particular, have utilized

* Corresponding author.
E-mail addresses: flases@hotmail.com (F. Lases-Hernandez), martin.medina@auburn.edu (M. Medina-Elizalde), sburns@geo.umass.edu (S. Burns), mrd0048@auburn.edu (M. DeCesare).

https://doi.org/10.1016/j.gca.2018.11.028
0016-7037/

paleoclimate observations to provide an empirical assessment of climate sensitivity and hydrological responses to shifts in the concentration of atmospheric greenhouse gases and other factors internal to the climate system (Palaeosens, 2012; Baldini et al., 2016; Medina-Elizalde et al., 2017). Stalagmite calcite oxygen isotope ($\delta^{18}O$) records represent one of the most important terrestrial paleoclimate archives of past hydrological variability in tropical and subtropical regions (Frappier et al., 2007b, 2014; Medina-Elizalde et al., 2010, 2016a, 2017; Fairchild and Baker, 2012; Kennett et al., 2012; Lachniet et al., 2012, 2017; Medina-Elizalde and Rohling, 2012; Akers et al., 2016; Cheng et al., 2016; Railsback et al., 2017). Hydroclimate records based on stalagmite $\delta^{18}O$ values are often interpreted to reflect the amount effect; the inverse relationship between rainfall amount and rainfall $\delta^{18}O$ described by Dansgaard (1964), which has been observed on seasonal and interannual time scales in low latitude regions (Vuille et al., 2003; Lachniet and Patterson, 2009; Medina-Elizalde et al., 2016a). The implicit assumption is that stalagmite calcite is deposited at or near isotopic equilibrium and that it preserves the variability of $\delta^{18}O$ of meteoric precipitation. This type of data collection requires a continuous commitment and expertise to access and work inside of a cave frequently enough and over an extended period of time. The evaluation of the rainfall/drip water isotopic relationship, nevertheless, is crucial when comparing isotopic variations within a single stalagmite and among different stalagmite $\delta^{18}O$ records and particularly if the goal is to reconstruct precipitation amount quantitatively (e.g. Medina-Elizalde et al., 2010; Lachniet et al., 2012, 2017; Medina-Elizalde and Rohling, 2012). The $\delta^{18}O$ composition of rainfall may be altered between the ground surface and cave drips due to isotopic fractionation in the soil, epikarst and/or vadose zone driven by evaporation (Ayalon et al. 1998; Bradley et al. 2010; Cuthbert et al., 2014; Beddows et al. 2016, Hartmann and Baker, 2017), and by mixing of water reservoirs in the epikarst (Yonge et al., 1985; Ayalon et al., 1998; Williams and Fowler, 2002; McDermott, 2004; Fairchild et al., 2006; Lachniet and Patterson, 2009; Genty et al., 2014; Hartmann and Baker, 2017). The resolution of a stalagmite $\delta^{18}O$-derived rainfall record, furthermore, is ultimately not determined solely by the stalagmite temporal sampling resolution, but by the time integration of the rainfall signal by drip water. Because of the type of porosity (Worthington and Ford, 2009) and spatial heterogeneity of the water reservoirs and conduits of the vadose zone in a limestone cave, drip water (and thus stalagmites) can potentially integrate the amount-weighted isotopic signal of rainfall accumulated over days (Luo et al., 2014; Duan et al., 2016), a season (Cruz, 2005; Cobb et al., 2007; Fuller et al., 2008; Genty, 2008; Beddows et al., 2016; Duan et al. 2016), a year or even multiple years (Yonge et al., 1985; Williams and Fowler, 2002; Onac et al., 2008; Riechelmann et al., 2011, 2017; Genty et al., 2014; Czuppon et al., 2018). Drip water information, therefore, is particularly relevant to studies with high-resolution stalagmite $\delta^{18}O$ sampling that seek to characterize seasonal or annual precipitation variability (Medina-Elizalde et al., 2010; Medina-Elizalde and Rohling, 2012; Kennett et al. 2012, Lachniet et al., 2012, 2017) and to discern the negative isotopic anomalies of tropical cyclones (Frappier et al., 2007b). Rainfall events such as subtropical monsoons and tropical cyclones are characterized by particularly low $\delta^{18}O$ compositions, but these events are short lived, lasting from days (cyclones) to a season (monsoons) (Lawrence, 1998, Lawrence and Gedzelman 1996; Gedzelman et al., 2003; Lachniet and Patterson, 2009; Lachniet et al. 2017; Vieten et al. 2018). Interpretations of stalagmite $\delta^{18}O$ variations in terms of monsoon intensity and tropical cyclone activity are, therefore, contingent upon the time integration of the rainfall isotopic signal by drip water.

This study characterized the isotopic composition of rainfall, drip water, and groundwater on a weekly basis, over three hydrological years, from three different chambers of the Río Secreto cave system located in the northeastern Yucatán Peninsula (YP). In addition, we also monitored the cave environment in these chambers, each with a different degree of isolation from the surface environment. This sustained research effort was motivated by improving hydrological interpretations from stalagmite $\delta^{18}O$ records and by enhancing our understanding of the link between precipitation amount and effective groundwater recharge in the YP. Río Secreto cave offered valuable stalagmite rainfall records, including two spanning the Classic and Preclassic Periods in Maya history and the Last Glacial Maximum (23–26 kyr ago) (Medina-Elizalde et al., 2016a, 2017). The monitoring results presented in this study help to better interpret paleoclimate information from stalagmites while guiding sampling protocols for stalagmites from the Río Secreto cave system and other similar karst environments. The authors of this study are currently reconstructing additional paleoclimate records from this cave.

2. FIELD SITE

2.1. Study site, cave system and climate

The YP has a distinctive annual cycle in precipitation characterized by the *Nortes*, *Dry* and *Rainy* seasons. The *Nortes* cold front season occurs between the months of November and February, the *Dry* season from March to May and the *Rainy* season between June and October. The *Rainy* season, also known as the *hurricane season*, has a bimodal distribution of precipitation with maxima during June and September and a precipitation drop between July and August, known as the midsummer drought (Magaña et al., 1999). Precipitation maxima in the YP occur during September when the Intertropical Convergence Zone reaches its northern most position and when the peninsula experiences the maximum tropical cyclone frequency. Regional models and the NCEP-NCAR Global reanalysis, indicate that the dominant source of moisture for the YP is the Caribbean Sea and is linked to the Caribbean Low Level Jet (CLLJ) (Vuille et al., 2003; Mestas-Nuñez et al., 2007; Muñoz et al., 2008; Karmalkar et al., 2011).

Río Secreto Cave (Secret River Cave) is a shallow horizontally developed karst cave with 42 km of surveyed

passages, located in the northeast of the YP in the State of Quintana Roo, Mexico (20° 35.244′N; 87° 8.042′W, Fig. 1A; Sprouse et al., 2017). The cave is 5 km south of the city of Playa del Carmen, and the main entrance is five km from the Caribbean coast. Daily guided tours are conducted in small section of the overall cave. The climate of the northeastern YP is sub-humid, with average annual temperature of 25.8 °C and a range of 21–30 °C in monthly temperatures at Playa del Carmen (14 years measured by government meteorological stations, i.e. CONAGUA). Average annual precipitation in Playa del Carmen is 1463 ± 280 mm and more than 70% of precipitation occurs during the rainy season from June to November (Medina-Elizalde et al., 2016b). Summer precipitation is sourced by onshore trade winds off the Caribbean, and tropical storms and cyclones that cross the YP. Winter precipitation comes from humidity-saturated cold fronts (Orellana et al., 2009).

The geology is a highly karstified Pliocene carbonate rising to only 20 m above sea level (López-Ramos, 1975). High bedrock permeability leads to very little runoff and hence the shallow aquifer is recharged only by direct infiltration of precipitation. Caves are common along a 100 km section of the Caribbean coast from Playa del Carmen and south to the town of Tulum, including Sac Actum the world's longest underwater cave system (www.caves.org/project/qrss/qrlong.htm). The Río Secreto cave system lies at and above the water table, with extensive semi-flooded passages, all frequently interrupted by 1–8 m diameter sinkholes that allow ventilation of the system. The exceptional karstification and high hydraulic conductivity of the aquifer result in a water table nearly at sea level, with a shallow hydraulic gradient in the range of 10^{-5} cm per km. (Bauer-Gottwein et al., 2011). The coastal semi-diurnal tides affect the Río Secreto water table up to several cm, while rapid recharge during heavy rainfall can cause a short-term rise of up to 1 m (McMonigal and Beddows, 2014).

2.1.1. Soil and epikarst composition

The ecosystem is a tropical dry forest subject to natural fires, as well as slash-and-burn agriculture practiced by the Maya. The current vegetation cover is young, possibly because the area is in a state of recovery after a forest fire ~20 years ago. The bedrock is composed of Pliocene-Pleistocene carbonates that retains much of its porosity, allowing water penetration in addition to the more rapid infiltration through small fractures and secondary porosity features. As already mentioned, surface run-off is rare. An "epikarst" has been described as the superficial part of karst areas, where tree roots and karst processes fracture and enlarge rock joints and cracks, creating a more

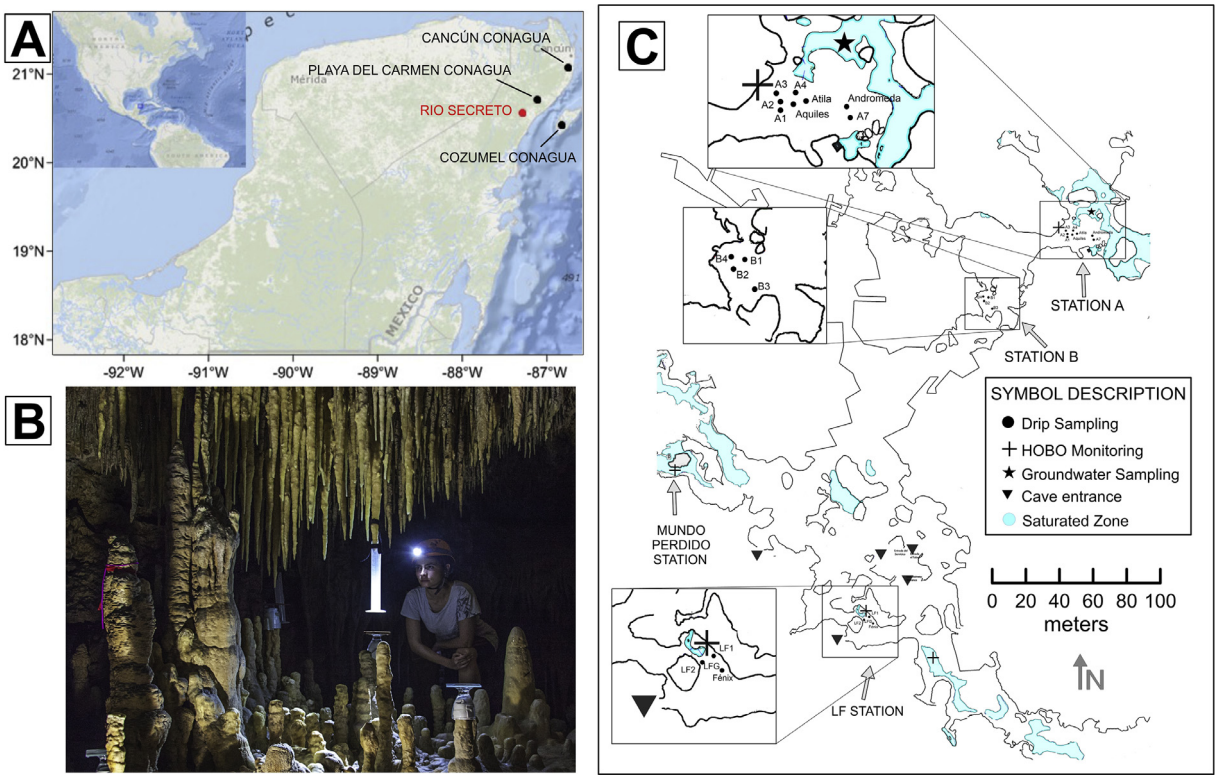

Fig. 1. (A) Location of Río Secreto cave (red dot) and of the government (CONAGUA) weather stations of Playa del Carmen, Cozumel and Cancún (black dots). (B) Station A, collection of drip water from A4 by hanging a graduated cylinder using Velcro. Visible also is a glass plate on top a stalagmite used to farm calcite. (C) Map of the monitored stations A, B and LF (modified from Sprouse et al. 2017). Note that "Corazón" chamber is off the map located ~350 m to the east from station A. (For interpretation of the references to colour in this figure legend, the reader is referred to the web version of this article.)

permeable and porous zone over less permeable massive carbonate rock (Bakalowicz, 2012). The vadose zone of Río Secreto cave and of most caves of northeast of YP fit this description and, therefore, all the processes described in this study are being carried out in the epikarst.

The soil above the cave is thin and variable, with pockets rarely reaching 0.5 m between areas of exposed bedrock. Because the roots and the soil penetrate into the bedrock, which is 2–12 meters thick, it is possible to observe them in the ceiling, walls and floor of the cave inside the vadose zone. Roots of some species use fractures to access moisture and the water table in the vadose zone. Some tree species have roots that can help develop or create small fractures that serve as conduits that increase the hydraulic conductivity (Bauer-Gottwein et al., 2011). Root respiration increases the amount of CO_2 in cave air (Cowan et al., 2013). Where porous carbonates are sub-aerially exposed during times of negative water budgets, shallow re-precipitation of carbonate forms slabs of indurated caliche or calcrete (also kankar and duricrust) (Bautista et al., 2011). Several layers of caliche at and above the water table have been documented along the Caribbean coast (Ward, 1985; Cabadas-Báez et al., 2010) and are likely present above Río Secreto cave. The local vadose zone also includes patches of friable fine-to-medium-grained carbonate, locally called sascab, which may also store water (Bautista et al., 2011). The patchy nature of the bedrock strata and consequently infiltration and storage, are expressed in the heterogeneity of the ceiling of the cave, where ceilings of some sections are decorated with hundreds of distributed stalactites, and conversely, other sections have ceilings devoid of water infiltration.

3. METHODS

3.1. Precipitation sampling and surface weather monitoring

A total of 36 monthly composite rainfall samples were collected over three years from June 2014 to June 2017. Rainfall samples were collected above the cave at ground level using HDPE 8-liter containers with a Ping-Pong ball over a funnel connected to a hose consistent with IAEA (2014) protocols. Rainfall samples were collected every week and their volume measured using a graduated cylinder. These samples were then aggregated into monthly samples from which an aliquot was taken for $\delta^{18}O$ and δD analysis. From June 2016, we installed a second pluviometer of the same design beside the first one, to collect when possible, samples of individual rainfall events that accumulated between 1 and 7 days. Ground-level precipitation at Río Secreto may underestimate the true rainfall amount due to the presence of dense vegetation potentially blocking lateral rainfall associated with large storms. Therefore, in this study we also examine the average of precipitation amount from June 2014 to July 2017 from weather station data from three other locales to compare with our rain gauge data; Playa del Carmen (20°37.200′N, 87 04.200′W), Cozumel Island (20°31.200′N, 86°57.000′W) and Cancún (21° 09,002′N, 86 ° 49,200′W) (See Fig. 1A). In order to estimate the historical recharge in Playa del Carmen we use precipitation amount and evaporation historical data from CONAGUA. Evaporation data was calculated using the Penmann-Montheit method (Allen et al., 1998).

3.2. Monitoring using data loggers

Monitoring of the cave chambers included measurements using HOBO Temperature/HR U23 data loggers of cave air relative humidity (RH) with accuracy ± 5% above 90% and air temperature (accuracy of ± 0.21 °C). Additional cave climate data was collected in the Corazón chamber, and water level data in the "Mundo Perdido" section of the cave (Fig. 1C). Cave air RH and temperature data were measured at 4 and 6-hour intervals from April 2012 to July 2017 in Station LF, Station A, and Corazón chambers (See Table 1 for more details). From July 2016 to January 2017 another HOBO Temperature/RH U23 was placed outside the cave under the shade 4 m from the ground and 20 m from the cave entrance to record at 3-hour intervals. Cave groundwater temperature 30 cm below the water table was determined at 1 hour intervals from November 2015 to July 2017 in Mundo Perdido and Station LF phreatic zones by using a HOBO Water Level U20L-01 data logger with accuracy of ±0.44 °C (see Fig. 1C and Table 1).

Daily average temperature data of January 2016 – June 2016 from a Davis Vantage Pro 2 station (accuracy of ±0.5 °C and 1% for RH) was used for this study, the station is located in the Planetarium of Playa del Carmen (20° 39.045′N, 87°5.208′W). An additional Davis Vantage Pro 2 weather station was installed in Río Secreto Nature Reserve above the canopy approximately midway between the coast and the cave main entrance in June 2016.

3.3. Groundwater and drip water monitoring

The monitored portion of the Río Secreto cave system is shown in Fig. 1C. Three chambers were selected as stations for the drip study: Laberinto del Fauno (LF), located close to an entrance and stations A and B located ~200 m from the nearest entrance. The vadose zone bedrock above these 3 chambers is 9–12 m thick. Groundwater sampling began in June 2014 and consisted of weekly measurements of temperature, pH and electrical conductivity at the water table of station A using a HACH multi-parameter probe pre-calibrated with buffer pH 4, 7 and 10 and a sodium chloride standard solution of 491 ± 2.5 mg/L (1000 ± 10 µS/cm) with accuracy of 0.1 for pH and 0.01 mg/L for TDS. Water samples were also collected in 30 mL Nalgene bottles at a depth of 30 cm for $\delta^{18}O$ and δD analysis. In addition, we selected 16 drip sites associated with stalactites known to be hydrologically active throughout the year to take drip water samples. Each drip was monitored quasi-weekly from June 2014 to June 2017. The sampling protocol in station LF included drip water from 3 individual stalactites labeled LF1, LF2 and Fénix, and an additional point combining drip water from several stalactites labeled LFG. At station A, drip water from 8 individual stalactites were monitored: A1, A2, A3, A4, A7, Andromeda, Aquiles and Atila. At station B, four individual stalactites were monitored: B1,

Table 1
Summary of temperature data from drips, groundwater and air (°C) inside and outside Río Secreto Cave system.

Station	Sample	Period	Frequency	n	AVG	SD	MIN	MAX
Corazón	Air	April 2012–May 2014	6 h	3104	24.8	0.0	24.7	24.9
	Groundwater	April 2012–May-14	3 h	6208	24.8	0.0	24.7	24.8
LF	Air	July 2014–July 2017	6 h	6840	22.8	1.2	18.8	24.5
	Air	July 2016–July 2017	6 h	1454	23.7	0.7	24.7	22.6
	Groundwater	Oct 2015–July 2017	1 h	13,867	22.8	0.9	20.7	24.1
	Drips	July 2014–July 2017	Weekly	270	23.0	1.9	18.2	24.8
A	Air	July 2014–July 2017	6 h	3616	24.5	0.2	23.8	24.9
	Air	July 2016–July 2017	6 h	1454	24.4	0.2	23.8	24.7
	Groundwater	Oct 2015–Nov-15	1 h	960	24.6	0.0	24.6	24.6
	Groundwater	July 2014–July 2017	Weekly	68	24.7	0.1	24.6	24.8
	Drips	July 2014–July 2017	Weekly	487	24.5	0.3	23.8	25.0
B	Drips	July 2014–July 2017	Weekly	232	24.6	0.3	24.6	24.8
Mundo Perdido	Groundwater	Dec 2015–Jul-17	1 h	12,902	24.2	0.4	23.0	24.7
Rio Davis Station	Air	July 2016–July 2017	6 h	1454	26.2	3.4	14.5	33.9

B2, B3 and B4. The monitoring periods for each drip span slightly different time intervals and only drips LF1, A3 and B1 were sampled continuously over the three-year period. Two of the selected chambers, LF and A, are sites where stalagmites have been collected (Medina-Elizalde et al., 2016a, 2017) and most of the 16 drips studied are above active candlestick stalagmites longer than 30 cm. A representative image of the monitoring and sampling sites is provided in Fig. 1.

For almost all drips (except LFG, A2 and LF2), drip water was collected by hanging a clean dry 250 mL plastic graduated cylinder from each stalactite using Velcro to ensure that no secondary drips were collected (see Fig. 1B). After the accumulation period (~48 h; See Table A.1), the volume of dripwater collected and its temperature were recorded, the latter, using a ThermoWorks digital thermometer (accuracy of ±1.0 °C). Then, sample aliquots were decanted into 15 mL and 30 mL Nalgene bottles for $\delta^{18}O$ and δD analysis. If the collected water volume was sufficient, pH and electrical conductivity were measured using the HACH probe. Drip rate is reported in mL/hr based on total volume divided by the collection interval. If the drip volume of a particular drip was greater than 250 mL and the water sample overflowed the cylinder drip rates were recorded as 8 mL/hr, thus representing a minimum flow but still allowing characterizing infiltration during significant rainfall events.

3.4. Stable isotopes

The $\delta^{18}O$ and δD values of groundwater, precipitation and drip water samples collected up to the year 2016 were determined using a Cavity Ring-Down Spectroscopy (CRDS) Picarro Isotope Analyzer, model L1102-i at the University of Massachusetts, Amherst. Reproducibility of in-house standard waters was better than 0.08‰ for $\delta^{18}O$ and 0.4‰ for δD. The $\delta^{18}O$ and δD analyses of groundwater, precipitation and drip water collected after 2016 were performed using a Cavity Ring-Down Spectroscopy (CRDS) Picarro Isotope Analyzer, model L2130-i at Auburn University, Alabama. Long-term reproducibility of in-house Picarro Zero and Mid standard waters in both labs was better than 0.03 ‰ for $\delta^{18}O$ and at 0.2 ‰ for δD. Results are reported in per mil (‰) relative to VSMOW (Vienna Standard Mean Ocean Water).

4. RESULTS

4.1. Temperatures and relative humidity

A summary of the cave air, dripwater and groundwater temperature data is presented in Table 1. During the period between July 2016 and July 2017 the total range of air temperature variation inside the cave was 1–2 °C while the total range observed outside the cave spanned 19 °C (Fig. 2). Groundwater, cave air and drip water temperature variability at station LF was the most pronounced of all the stations. Observed mean annual air temperature outside the cave and at LF and A stations was the same, although the daily air temperature range inside the cave was only a small fraction (<12%) of that observed outside (July 2016-July 2017) (Table 1, Supplementary Fig. A.1). Seven months of air temperature data collected at 12 h. intervals inside LF and outside the cave indicate that LF follows atmospheric temperature variability within an hour. As noted above, however, LF greatly buffers the atmospheric air temperature range (Supplementary Fig. A.1). Cave drip water and air temperature at stations A and LF were similar, reflecting thermal equilibrium within a 48-hour period maximum (Supplementary Table A.1 and Fig. 2)

Río Secreto surface air RH averaged 84% with a range of 68% to 98% during 2016 and 2017. RH at LF station ranged from 89.9% to 100%, with an average of 99.9 ± 0.8% (n = 5106). At station A, RH ranged from 95.3% to 100%, with average of 99.6 ± 0.9% (n = 3616) (Fig. 2). Considering the small uncertainty associated with RH measurements (5%), all the chambers investigated exhibit water vapor saturation conditions.

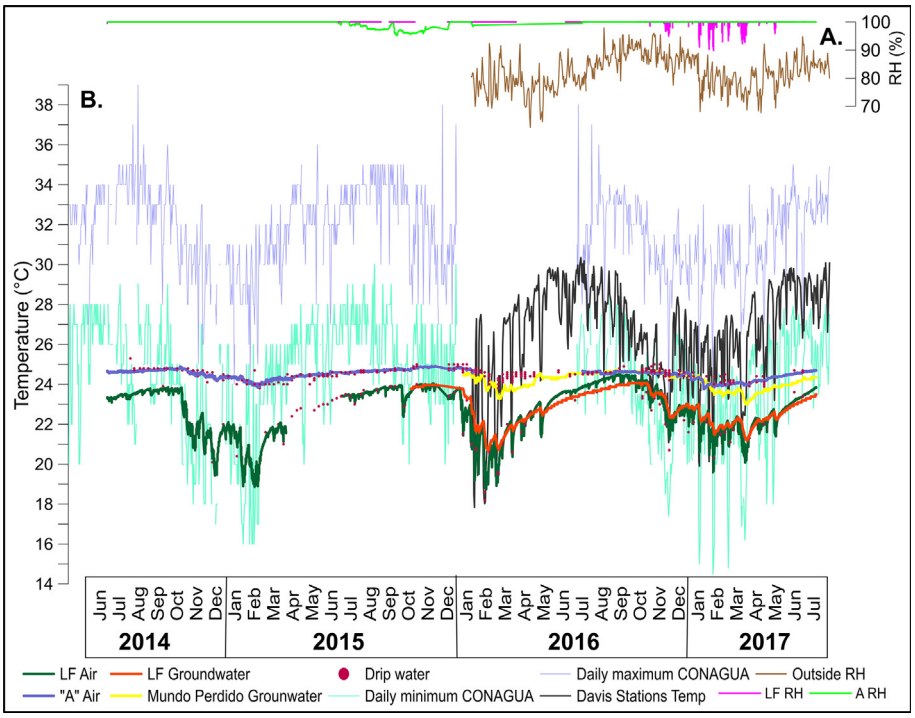

Fig. 2. (A) Air relative humidity recorded outside and inside Río Secreto cave. (B) Temperatures outside the cave: Daily record of maximum, and minimum temperatures in Playa del Carmen measured by CONAGUA and daily average temperatures measured by two Davis Vantage Weather Stations (See Section 3.2). Cave groundwater, drip water, and air temperatures at stations LF, A and "Mundo Perdido" (see Section 3.2). Note minimum temperature variability within isolated chambers of stations A and "Mundo Perdido" that contrast with the more significant temperature variability at station LF, located near an entrance. The temperature range in station LF is smaller (~6 °C) relative to surface air (19 °C). Mean summer temperatures at station LF approximate temperatures in the isolated chambers of stations A and "Mundo Perdido".

4.2. Precipitation $\delta^{18}O$ and δD

A total of 66 samples of rainfall were analyzed for $\delta^{18}O$ and δD, including monthly samples (n = 36) and samples of individual rainfall events (n = 30) (Figs. 3 and 4, Supplementary Fig. A.2). This sample collection included a particularly intense rainfall event on October 21, 2014, representing an accumulation of 150 mm/day, which had the lowest isotopic values found in this study ($\delta^{18}O = -9.5‰$, $\delta D = -61.4‰$). This study includes the drought year of 2016, when annual precipitation was 40% lower than the long-term average and nearly half that of the previous year.

Rainfall $\delta^{18}O$ and δD varied from −9.5‰ to +1.5‰ and from −61.4‰ to +17.9‰, respectively (n = 66) (Fig. 4). Monthly rainfall $\delta^{18}O$ and δD ranged from −7.4‰ to −0.6‰ and from −45.8‰ to 12.3‰, respectively (n = 36; Fig. 4). The amount-weighted mean isotopic compositions of rainfall calculated from monthly data (n = 36) were −3.7‰ and −17.8‰ for $\delta^{18}O$ and δD, respectively. The amount-weighted annual $\delta^{18}O$ composition of rainfall over the study interval, was −4.2‰ (yr. 1), −4.5‰ (yr. 2) and −2.3‰ (yr. 3). The arithmetic average (not amount-weighted) based on monthly samples (n = 36) was −2.6‰ and −9.3‰ for $\delta^{18}O$ and δD, respectively (Table 2). We stress here, that the arithmetic mean does not truly represent the annual $\delta^{18}O$ composition of rainfall because it weighs all months the same regardless of their relative contribution to the total annual rainfall amount. We include this calculation, however, because it represents one potential end-member of the mean annual drip water $\delta^{18}O$ composition, also estimated without weighing water amounts. More details are provided below.

A negative relationship between precipitation amount and precipitation $\delta^{18}O$ (i.e. an amount effect) is revealed by our precipitation data on seasonal timescales, as expected in tropical regions (Dansgaard, 1964; Rozanski et al., 1993; Lachniet and Patterson, 2009). The slope of the amount effect relationship in Río Secreto is −0.0142 ‰mm^{-1} ($r^2 = 0.6$) (Fig. 4), very similar to observations from Veracruz, México, and El Salvador; −0.0125 ‰mm^{-1} and −0.0124 ‰mm^{-1}, respectively (Lachniet and Patterson, 2009).

4.3. Groundwater level and isotopic composition

The average $\delta^{18}O$ and δD values of groundwater in Río Secreto cave were $-4.7 \pm 0.1‰$ (1 standard deviation, SD) and $-25.5 \pm 0.9‰$ (1 SD), respectively, from July 2014 to July 2017 (n = 78 samples). The $\delta^{18}O$ value of groundwater was within analytical uncertainty of the annual amount-weighted $\delta^{18}O$ composition of rainfall observed in the three-year study period (−4.5‰ to −2.3‰), and the most temporally stable of all the water types analyzed, suggesting

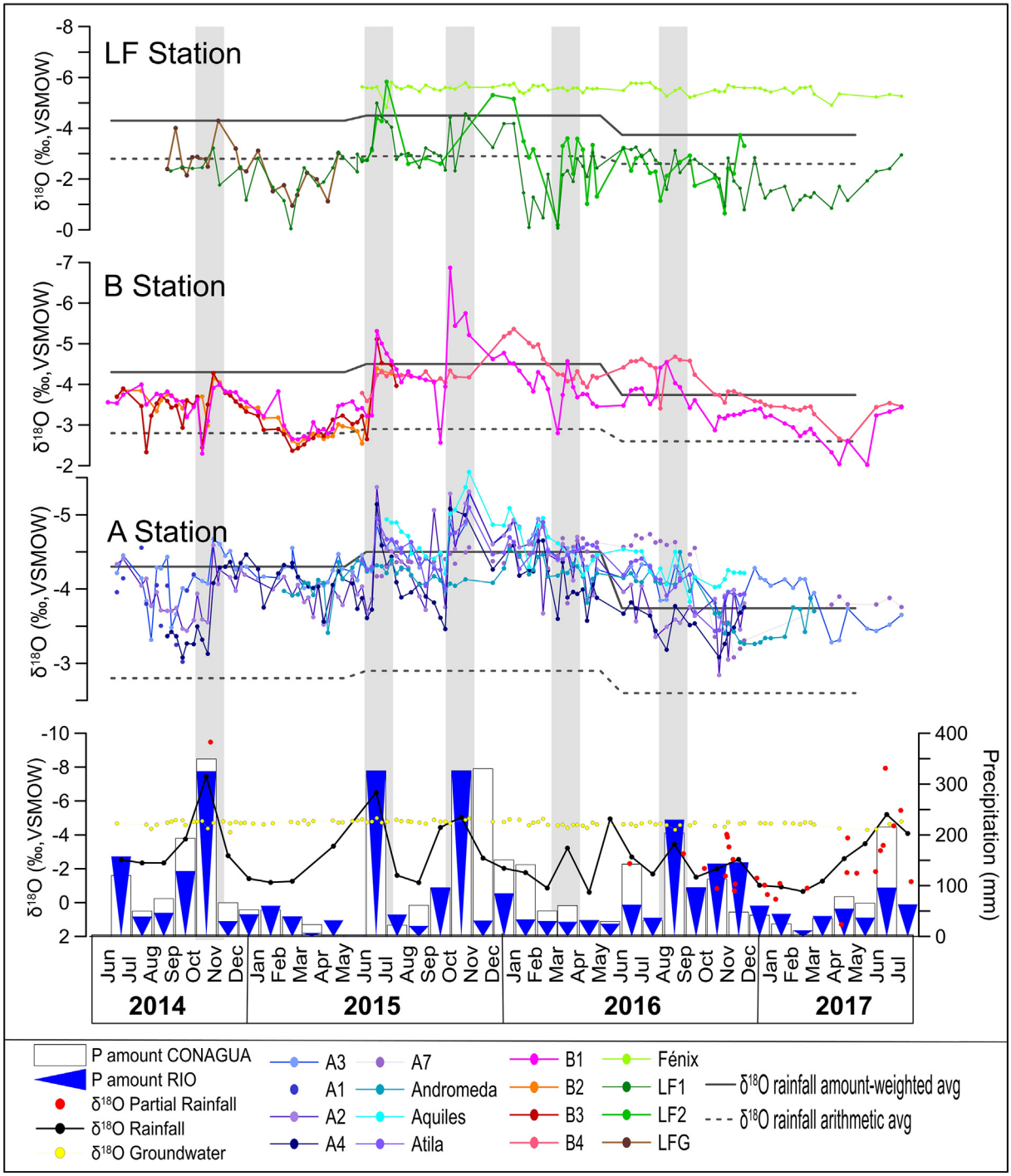

Fig. 3. Upper three panels: drip water $\delta^{18}O$ data from June 2014 to June 2017 from stations LF, B and A; Note that axes are inverted. Lower panel: (blue triangles) monthly precipitation collected at the location of Río Secreto cave; (white rectangles) monthly precipitation recorded by CONAGUA, including weather stations in Cancún, Playa del Carmen and Cozumel; (black line) precipitation $\delta^{18}O$ from monthly samples, and; (red dots) individual rainfall events (1–7 days) (See Section 3.1). $\delta^{18}O$ Annual amount-weighted and arithmetic averages of rainfall are shown to ilustrate two end members (See Sections 4.4 and 5.2). Gray bars highlight conspicuous drip $\delta^{18}O$ shifts coeval with rainfall $\delta^{18}O$ changes. (For interpretation of the references to colour in this figure legend, the reader is referred to the web version of this article.)

it represents the integration of about one or more years of rainfall accumulation (Fig. 3, Supplementary Fig. A.2). Groundwater is actively moving through Río Secreto, probably toward the ocean, as mentioned in Section 2.1, water table is affected by the coastal semi-diurnal tides and recharge (McMonigal and Beddows, 2014).

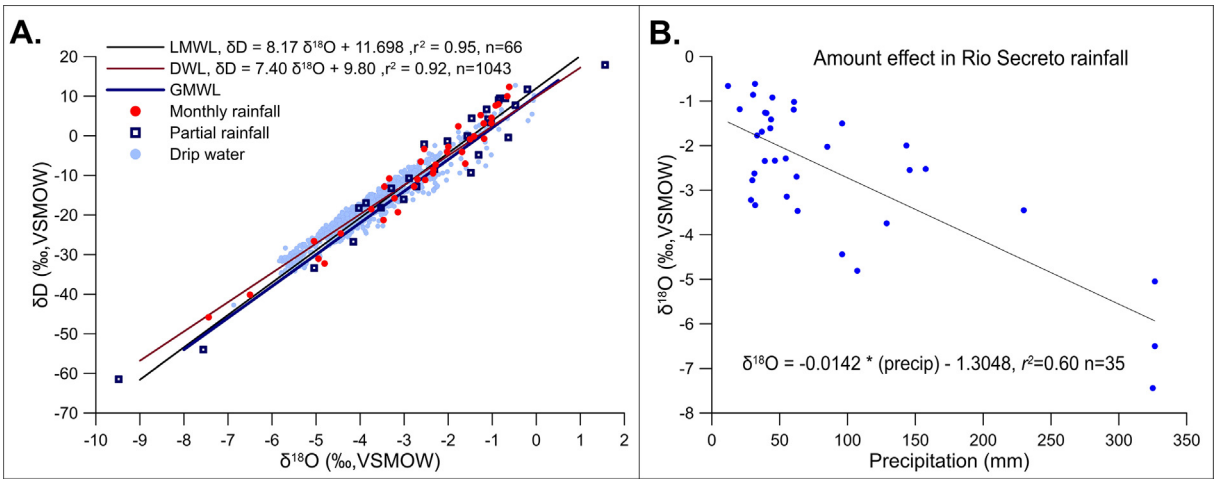

Fig. 4. A. Comparison of the linear relationship between $\delta^{18}O$ and δD of monthly rainfall samples and samples of individual rainfall events (local meteoric water line, LMWL), and drip waters (drip water line, DWL) of Río Secreto cave. The global meteoric water line (GMWL) is also shown to provide global context. B. Linear relationship between $\delta^{18}O$ and monthly rainfall amount collected in Río Secreto. Both plots present data collected from June 2014 to July 2017.

Table 2
$\delta^{18}O$ and δD averages and standard deviation of monthly rainfall, drips and groundwater collected from June 2014 to July 2017.

Sample description	n	$\delta^{18}O$				δD			
		AVG	SD	MIN	MAX	AVG	SD	MIN	MAX
Monthly Rainfall									
Arithmetic	36	−2.6	1.6	−7.4	−0.6	−9.3	13.9	−45.8	12.3
Amount-Weighted	36	−3.7				−17.8			
A1	11	−3.9	0.4	−4.6	−3.0	−19.6	2.7	−22.8	−13.5
A2	94	−4.1	0.5	−5.4	−2.8	−20.4	4.0	−30.1	−9.0
A3	113	−4.2	0.4	−5.3	−3.3	−21.6	2.7	−27.5	−15.2
A4	83	−3.9	0.5	−5.1	−3.1	−19.5	3.5	−29.3	−11.1
A7	62	−4.3	0.4	−4.8	−3.1	−21.9	3.9	−26.9	−12.1
Andrómeda	79	−4	0.3	−4.5	−3.3	−19.7	2.8	−25.4	−13.5
Aquiles	47	−4.5	0.4	−5.6	−3.8	−24.1	2.4	−29.7	−17.9
Atila	56	−4.4	0.3	−5.1	−3.4	−22.6	2.9	−26.3	−13.9
B1	115	−3.6	0.8	−6.9	−2.0	−16.6	5.9	−42.7	−6.0
B2	42	−3.3	0.5	−4.4	−2.5	−13.7	4.5	−24.3	−6.5
B3	44	−3.3	0.6	−5.1	−2.3	−13.9	4.8	−27.8	−4.8
B4	69	−4.1	0.6	−5.4	−2.6	−20.5	4.8	−30.5	−11.3
Fénix	72	−5.5	0.2	−5.8	−4.8	−32.0	1.8	−35.1	−25.6
LF1	94	−2.4	1	−5.0	0	−7.9	8.0	−27.3	12.7
LF2	41	−2.8	1.2	−5.8	−0.2	−12.7	7.5	−31.6	4.3
LFG	21	−2.4	0.9	−4.3	−1.0	−7.2	6.4	−20.2	5.6
Total Drips	1043	−3.9	1	−6.9	0	−18.9	7.4	−42.7	12.7
Groundwater	101	−4.7	0.15	−5.0	−4.2	−26.0	1.4	−28.4	−19.5

4.4. Drip water $\delta^{18}O$ and δD

A total of 1043 samples from 16 different drip sites were analyzed for $\delta^{18}O$ and δD (Supplementary Table A.1, Fig. 3 and Fig. A.2). This study examines the annual average and amplitude $\delta^{18}O$ variability of drips, because of its application to hydroclimate reconstructions from speleothems. We note that the annual $\delta^{18}O$ composition of drip water of each site is not from samples that are amount-weighted because our sampling protocol involves the collection of temporally discrete water samples that represent aliquots from a reservoir of unknown size. Thus, the annual mean drip water $\delta^{18}O$ composition that we determine is not expected to perfectly represent the $\delta^{18}O$ composition of all the drip water that actually drained over the course of a year. This is analogous to estimating the annual $\delta^{18}O$ composition of rainfall from monthly precipitation $\delta^{18}O$ data without taking into account the monthly amount of rainfall: this calculation would not provide the true annual $\delta^{18}O$ composition of rainfall over the course of that year. We anticipate, therefore, that our sampling protocol would yield a drip annual mean $\delta^{18}O$ composition more closely

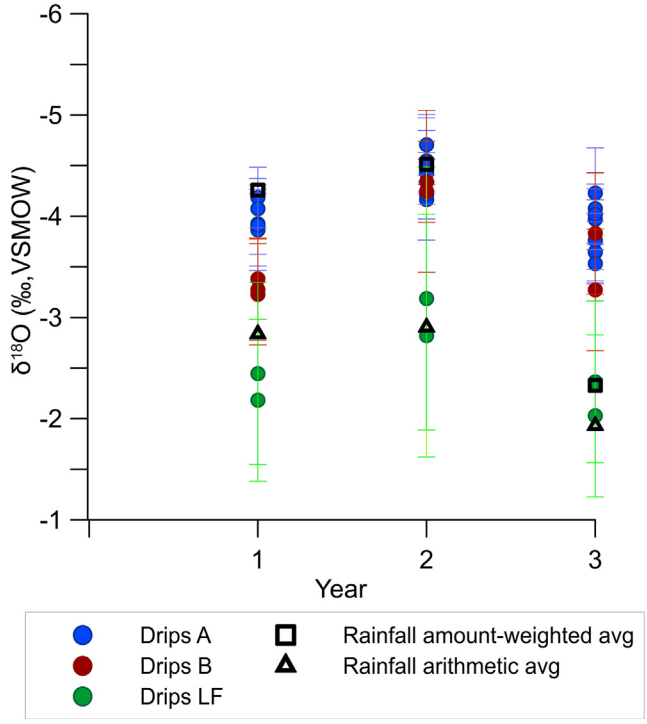

Fig. 5. Río Secreto amount-weighted and unweighted (arithmetic) annual drip water and rainfall $\delta^{18}O$ data; Note that axis is inverted. Values were calculated from June 2014 to May 2015 (year 1), June 2015 to May 2016 (year 2) and June 2016 to May 2017 (year 3). Only drip data with more than 15 data points per year were included (see Supplementary Table A.3). Drips at station A have a similar isotopic composition to the amount-weighted $\delta^{18}O$ composition of rainfall during year 1 and 2. Drips at station B have an isotopic composition in between the amount-weighted and unweighted $\delta^{18}O$ composition of rainfall. Lastly, drips at station LF have an isotopic composition similar to the mean $\delta^{18}O$ composition of rainfall, unweighted. During year 3 the YP experienced a drought reflected by a positive shift in the isotopic composition of rainfall (black triangle and square shown in year 3). Bar errors of 1 SD are showed for drip waters.

resembling the annual arithmetic mean $\delta^{18}O$ composition of rainfall (i.e. amount-unweighted) when a drip integrates rainfall over a short time. Conversely, a drip annual mean $\delta^{18}O$ composition resembling the annual amount-weighted $\delta^{18}O$ composition of rainfall would be indicative of a reservoir that accumulates rainfall for one year. We note, furthermore, that drip sites that integrate one year of rainfall are expected to show a modest response to rainfall $\delta^{18}O$ variability and thus minor $\delta^{18}O$ variability during the year. We find drips that fall within these two annual isotopic end members as described below.

4.4.1. Station A

With the exception of Fénix, the drip sites with the smallest annual $\delta^{18}O$ variability (~2‰) were those at station A (Figs. 3 and 5). The annual mean $\delta^{18}O$ composition of these drip waters closely resembles the annual amount-weighted $\delta^{18}O$ composition of rainfall during years 1 and 2 (Fig. 5). During year 3, drip waters at station A display lower $\delta^{18}O$ values than coeval rainfall, and closely resemble the isotopic composition of rainfall in the previous year (Fig. 5).

4.4.2. Station B

The mean annual $\delta^{18}O$ composition of drips from station B had values between the annual amount-weighted and unweighted $\delta^{18}O$ composition of rainfall during year 1, and similar to the annual amount-weighted $\delta^{18}O$ composition of rainfall during year 2. Similar to drip waters at station A, during year 3, the mean annual $\delta^{18}O$ composition of drip water at station B is more negative relative to that of rainfall (both amount-weighted and unweighted), and similar to the $\delta^{18}O$ mean composition of rainfall in the previous year (Fig. 5). Drip waters from station B show larger $\delta^{18}O$ variability during 2015 (~4‰) than during 2014 and 2016 (~2–3‰).

4.4.3. Station LF

Drip Fénix at station LF had the lowest isotopic values and lowest temporal variability of all drip waters ($\delta^{18}O = -5.5 \pm 0.2$‰) (Fig. 3, Table 2). Fénix has $\delta^{18}O$ values that range from −5.8 to −4.8‰ and are up to ~2‰ lower than the annual amount-weighted $\delta^{18}O$ composition of rainfall (-3.7 ± 1‰, n = 3 years). Drips LF1 and LF2, from the same chamber, in contrast, show the largest $\delta^{18}O$ variability (~6‰) of all the drips examined in this study. LF1 and LF2 $\delta^{18}O$ variability (~6‰) closely resembles that of rainfall over the same time interval (9‰) (Fig. 3 and Fig. A.3). It is notable that these drip sites are located only 5 m away from Fénix (Fig. 1C). The mean annual $\delta^{18}O$ compositions of LF1 and LF2 are close to the mean $\delta^{18}O$ value of rainfall (unweighted) during all three years (Fig. 5).

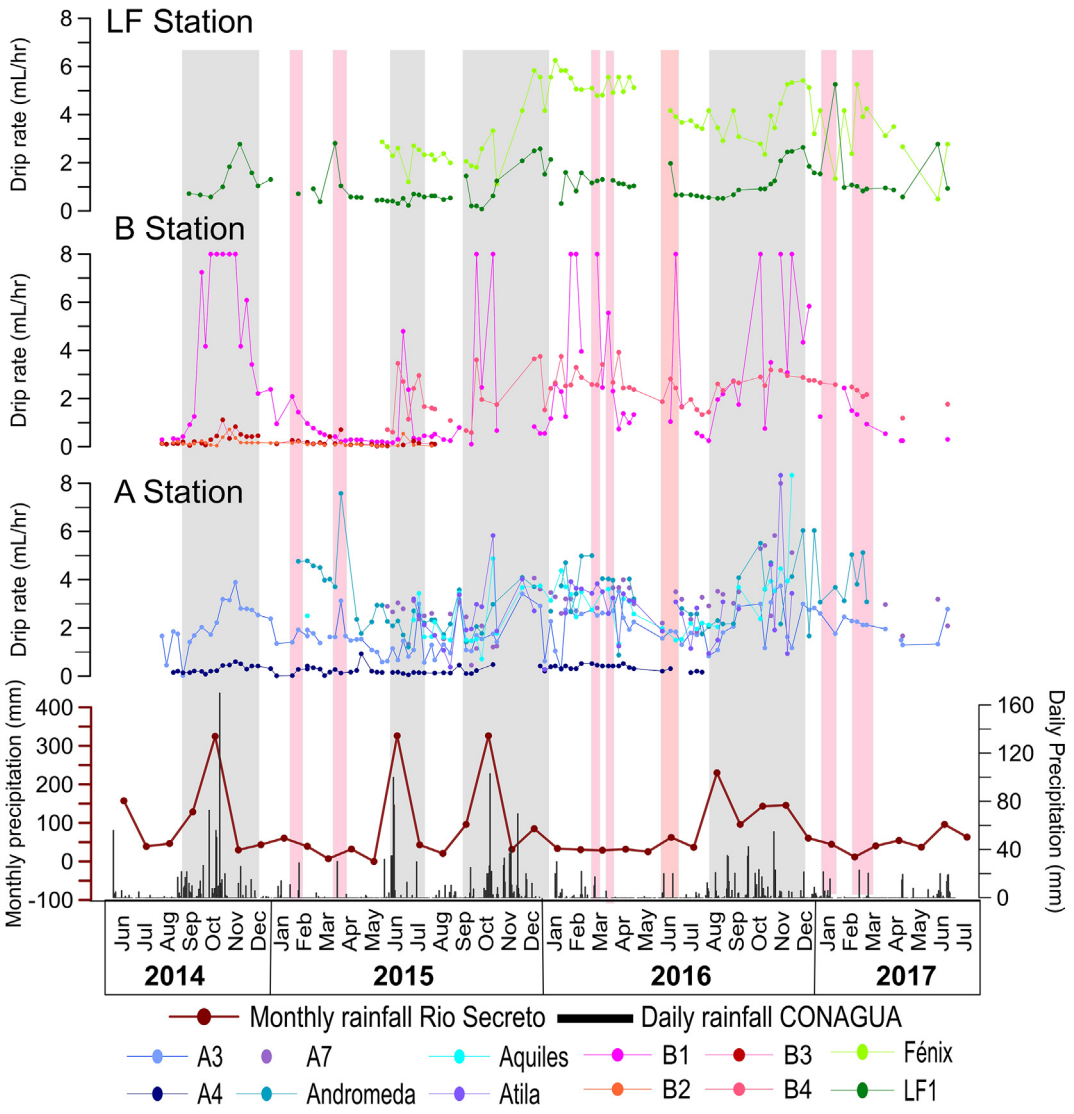

Fig. 6. Upper Panel: Drip rate in mL/hr at stations LF, B and A. Lower Panel: Monthly rainfall amount collected near the main entrance of Río Secreto cave (red line) and daily rainfall amount recorded by CONAGUA (2017) in Playa del Carmen. Gray bars highlight drip rate increases during the rainy season. Pink bars highlight drip rate increases in response to individual rainfall events. (For interpretation of the references to colour in this figure legend, the reader is referred to the web version of this article.)

4.5. Discharge variability of cave drips

In order to examine the infiltration of rainwater into the karst system and its relationship with the isotopic composition of drip water, drip rates were determined throughout the three-year monitoring effort. Drip rate variability ranged from 0.01 mL/h. to more than 16 mL/h, including all drips (Supplementary Table A.1). Despite discharge rates increasing in most drips during the rainy season, marked differences among them were observed (Fig. 6). In some cases, an increase in drip discharge immediately followed individual rainfall events (e.g. Drips B1, A3, Fénix). However, other drip discharge lagged rainfall amount shifts by a few weeks and to three months (e.g. Drips A7, Andromeda, Aquiles and Atila). We note that a similar lag between drip discharge and rainfall amount has been documented for Río Secreto cave at station A, via a calibration study of automatic drip sensors (Beddows and Mallon, 2018).

We determined the hydrological behavior of the drips using the maximum discharge and the coefficient of variation (i.e. the quotient of the standard deviation over the mean drip rate value expressed as a percentage) of the discharge according to the classification of Fairchild et al. 2006 (Fig. 7). We found that several of the drips that maintain a high and temporally constant drip rate seasonally can be classified as Seepage flow (e.g., A7, Andromeda, B4, Fénix, A3). Atila, Aquiles, A4, B1, B2, B3 and LF1 drips are classified as Seasonal Drips, i.e. drips that have both the lowest and highest drip rates of those examined. We note that the observed drip rate variability associated with B1 was distinct from all the other drips which suggests a threshold response to rainfall amount, as an "overflow"

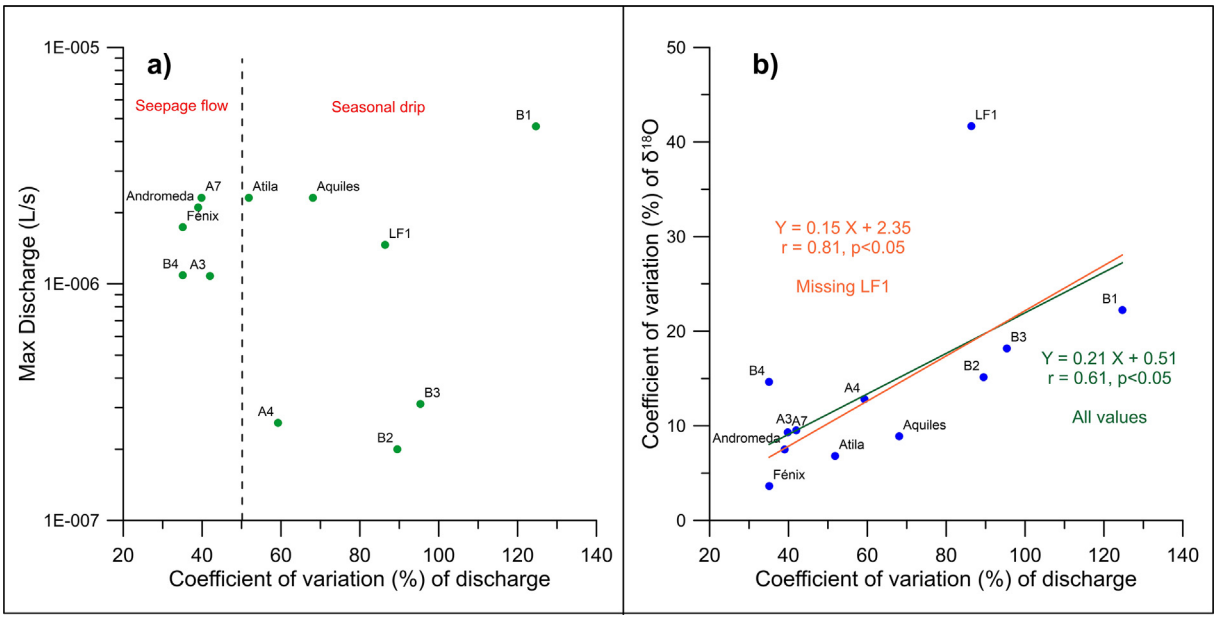

Fig. 7. (a) Hydrological behavior of Rio Secreto cave drip sites expressed in terms of maximum discharge versus variability in discharge defined by Fairchild et al. (2006). (b) Comparison between drip $\delta^{18}O$ and discharge rate variability. All data correspond to the period between July 2014 and July 2017.

drip (Smart and Friederich, 1987; Arbel et al., 2010; Bradley et al., 2010).

5. DISCUSSION

5.1. Temperature and cave ventilation

The observed modest variability of cave air, dripwater and groundwater temperatures at stations A and B is consistent with their isolation from the cave exterior. There is no difference between mean cave air and mean surface air temperatures (Fig. 2), reflecting the thermal equilibrium with surface heating by conduction (Smerdon et al., 2003), as has been reported in many caves around the world (Rau et al., 2015). Temperature variability in LF Station (groundwater, air and drip waters) in contrast with the isolated chambers (stations A and B) is more pronounced and closely follows seasonal air surface temperature variability, although with an amplitude modulation (Fig. 2 and Supplementary Fig. A.1.). An amplitude-modulated response of cave air temperature to surface air temperature may result from the "chimney effect"; the predominant effect of seasonal air circulation within a cave with two or more entrances. Cave temperature is expected to be constant over the course of a year in a closed environment, but variable when the cave is open to surface air. In this case, differences of temperature and air density between the surface and cave environments drives cave ventilation due to pressure disequilibrium (Wigley and Brown, 1976; Oh and Kim, 2011). Ventilation in Río Secreto cave is enhanced during the winter season, when the surface-to-cave air temperature contrast increases, thus cooling the cave. Due to the high heat capacity and thermal inertia of groundwater relative to air within the cave, its temperature variability is more modest (~3 °C) than air temperature (~6 °C). We note that later in the summer when the highest air surface temperature is reached (~34 °C), LF reaches a maximum air temperature similar to the annual mean temperature observed in the more isolated chambers (24.5 °C). Temperature in LF station does not increase beyond this point and does not reach typical, higher peak summer surface air temperature because it becomes thermally isolated like stations A and B. "Mundo Perdido" is another section of the cave that represents temperature variations between LF and the isolated chambers A and B. This chamber is located near an opening to the surface but not as close as LF is from a similar opening (Fig. 1). Groundwater at this location, as expected, shows larger temporal temperature variability than the isolated chambers but lower than station LF (Fig. 2, Table 1). Comparing coeval air temperatures at LF and A stations and outside temperature measured using data loggers, we find that cooling by ventilation is occurring also on a daily basis; we did not detect a lag in the temperature cave-surface coupling (Fig. A.1. Supplementary). In some caves temperature changes have been related to visitations (Baldini et al 2006; Frisia et al., 2011; Vieten et al., 2016), but the close coupling between surface air and cave temperatures and the minimum annual variability at station A does not support this scenario for Río Secreto (Table1, Fig. 2 and Fig. A.1. Supplementary). Río Secreto cave represents over 40 km passages, and tourist activity in the system consists of about 12 visitors at a time traversing about 1 km of cave, and rarely spending more than 5 minutes in any chamber of the system.

5.2. Infiltration and transmission of the rainfall isotopic signature

Due to the thin ~10 m permeable vadose zone above Río Secreto cave, infiltration of rainfall from the surface to stalactites (drip waters) occurs rapidly, as suggested by our isotopic and discharge data. Different infiltration patterns, however, are observed among and within the 3 studied chambers. Because drip water data represents a brief interval of time (~48 h, every one or two weeks), we cannot calculate an annual amount-weighted isotopic composition for each drip and directly assess the degree to which drip water integrates the rainfall amount and isotopic signals, as mentioned previously. We observed, however, that the isotopic composition of drip water has annual values that fall between two end members: (1) drip waters whose annual mean $\delta^{18}O$ values are close to the annual amount-weighted $\delta^{18}O$ composition of rainfall, and; (2) drip waters whose annual mean $\delta^{18}O$ values are close to the arithmetic average isotopic composition of rainfall (amount-unweighted). Drip waters from stations A, B and LF fall at or within these two end members. Fénix seems to be an exception and is discussed in more detail below.

When considering discharge rates, we find that changes in drip flow and drip isotopic values are not always coeval with rainfall changes even within an individual drip site. For instance, the isotopic composition and drip rates of LF1 and B4 peaked at the same time in association with some rainfall amount maxima events, but lagged other similar rainfall events by weeks (e.g. June 2015) to months (e.g. October 2015) (Figs. 3 and 6). We find a significant correlation between the total variability of drip discharge and $\delta^{18}O$ composition ($r = 0.61$, $p < 0.05$). LF1 is a particular case that has significant variability of both drip rate and $\delta^{18}O$ values in comparison with the other drips. Removing the information from this drip, yields a more significant correlation ($r = 0.81$, $p < 0.05$) (Fig. 7) between drip rate and $\delta^{18}O$ variability: the greater the drip rate variability, the greater the associated $\delta^{18}O$ variability. In karst systems drips are fed by a combination of preferential flows (fissure and conduit) and through the matrix (seepage) converging between discrete water storages (Bradley et al., 2010). As a result of the complexity of the conduits through which water infiltrates and flows, water feeding each drip has a specific seepage behavior even when drips are only a few meters apart, such as in the case of Fénix and LF1 and LF2 (See Section 4.5).

Fig. 8 shows our proposed conceptual models to illustrate the different flow patterns as a function of reservoir size and infiltration flow, at stations A, B and LF. These conceptual models seek to explain drip rate and isotopic observations, as explained in more detail below.

Drip waters at station A integrate at least a year of rainfall accumulation and this reflects a larger epikarst water reservoir relative to the other two stations (Fig. 8). This inference is supported by the observation of modest annual drip $\delta^{18}O$ variability relative to that of rainfall and an annual mean $\delta^{18}O$ composition resembling the annual amount-weighted $\delta^{18}O$ composition of rainfall during years 1 and 2 (Fig. 5). The drips of station A are classified as both seepage and seasonal flow, with maximum drip rates above 10^{-6} (L/s). An exception is A4, which seems to be fed by matrix flow (Figs. 7 and 8).

At station B, drip waters show larger isotopic variability than at station A and an annual $\delta^{18}O$ values that fall between the annual amount-weighted and unweighted mean $\delta^{18}O$ composition of rainfall, during years 1 and 2 (Fig. 5). This suggests an integration of rainfall accumulation of few months and less than a year, suggesting a smaller reservoir than at station A (Fig. 8). We also note that differences in reservoir effects are observed within B station drips. Drips B4 and B1, for instance, located 1 meter apart, show a consistent $\delta^{18}O$ difference of about 0.5‰. B4 also presents marked differences in drip rate variability in comparison with B1, B2 and B3, suggesting they are associated with two different reservoirs (Figs. 3, 7, 8 and Table 2).

At station LF, with the exception of Fénix, drip waters show the largest isotopic variability, closely reflecting that of rainfall, with an annual $\delta^{18}O$ composition similar to the mean $\delta^{18}O$ composition of rainfall (unweighted). These observations suggest an integration of few weeks of rainfall accumulation, thus reflecting the smallest water reservoir of all stations. As expected, during year 3 when the YP experienced a drought, the only drips that capture the high rainfall $\delta^{18}O$ values associated with this drought are those from station LF (Fig. 5). Conversely, drip waters from stations A and B reflecting a larger integration time and, therefore, a larger water reservoir size, show more isotopic 'inertia' to a rainfall isotopic shift. This isotopic inertia is clearly expressed in year 3, when the $\delta^{18}O$ values of these drip waters increase by ~0.5 per mil relative to the previous year, despite the ~2 per mil positive change in precipitation $\delta^{18}O$ associated with this drought (Fig. 5). Drip waters that resemble the monthly and seasonal isotopic variability of rainfall have been found in previous studies but with a greater degree of amplitude modulation than it is observed in this study (Li et al., 2000; Cruz, 2005; Cobb et al., 2007; Luo et al., 2014; Beddows et al., 2016; Duan et al., 2016).

Results from Fénix, located ~5 m from LF1, LF2 and LFG, show the smallest flow rate variability and the lowest average isotopic values of all drip waters (Figs. 3, 7 and Table 2). Fénix drip rates suggest a discharge flow coeval with seasonal rainfall changes, but its mean isotopic values are 1 to 2‰ lower than the annual amount-weighted $\delta^{18}O$ composition of rainfall. Constant isotope composition of Fénix reveals that the residence time of its reservoir is greater than three hydrological years, and it is likely a very large reservoir with few discharge points. Drip waters with constant $\delta^{18}O$ that can have variable discharges have been documented and result from a complicated system of infiltration flows that always have a long water residence time (Duan et al. 2016). We propose that the low permeability of the epikarst above Fénix allows primarily infiltration only of intense rainfall events that exceed a certain volume threshold. Observed rainfall $\delta^{18}O$ values associated with intense rainfall events are sufficiently negative to explain Fénix's low isotopic values (Fig. 4). However, it is possible that due to this low permeability the water that infiltrates during any rainfall event does not have enough volume to significantly modify the isotopic signature of a very large

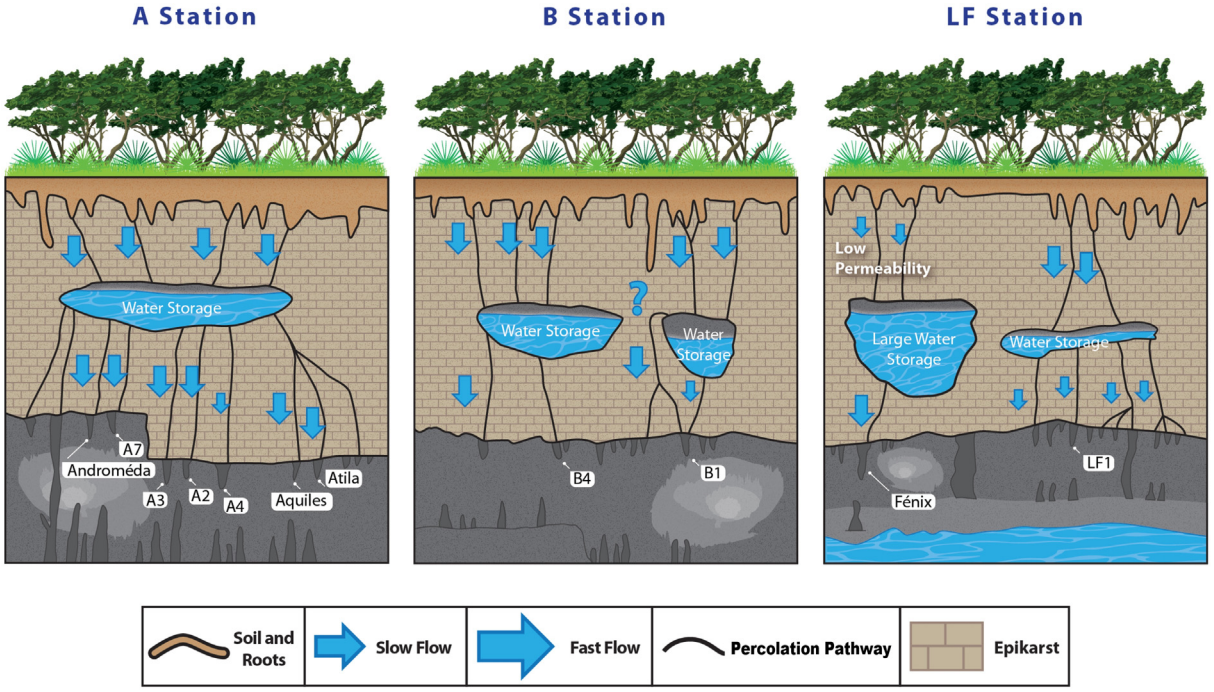

Fig. 8. Río Secreto conceptual model of infiltration of rainwater through the karst vadose zone at stations A, B and LF (modified from Hartmann and Baker, 2017). This was constructed based on drip rate and isotopic responses of the most widely monitored drips on a quasi-weekly time scale, from August 2014 to July 2017 (Table 2). We consider the infiltration pathways as a combination of matrix flow (i.e. slow flow) and preferential flow (i.e. fast flow) between discrete water storages. Station A is suggested to have a relatively large reservoir since its drips have average isotopic values very close to the annual amount-weighted $\delta^{18}O$ composition of rainfall. Station LF is proposed to have two reservoirs: the smallest one with discharge points for LF1; the drip that most closely resembles the isotopic amplitude of rainfall (Fig. A.2), and; the largest reservoir with few discharge points that supply Fénix, the drip with constant isotopic signature that preferably allows the infiltration of very low isotopically events (intense rainfall events). We propose at least two different reservoirs for station B: one reservoir associated with B4 that behaves similar to the reservoir of station A, and one reservoir for B1 the drip that shows a threshold response to rainfall amount; an overflow drip (see Section 4.2).

reservoir such as the Fénix reservoir, so it remains constant. Comparing with the other drip waters, the coefficient of variation of discharge and $\delta^{18}O$ both are very low at Fénix (35% and 4%, respectively; Fig. 7). This result implies that amongst all drip waters studied at Río Secreto cave, Fénix is the only one whose stalagmite does not reflect the annual or sub-annual rainfall variability, but would likely integrate several years of rainfall.

5.2.1. Deuterium excess variability

The deuterium excess defined by Dansgaard (1964) as d-excess = $\delta D - 8 * \delta^{18}O$, is a value that depends on the temperature and relative humidity in the moisture source region (Merlivat and Jouzel, 1979). Fig. 9 shows that the d-excess of the local rainfall at Río Secreto has a variability that is not controlled by temperature but likely controlled by the contributions of moisture from different sources on seasonal and interannual timescales. For instance, most of the rainfall that falls in this region originates from the tropical Caribbean with an influence also from the Tropical Pacific (Vuille et al., 2003). However, there are other contributions from the North Pacific that can modify the isotopic signature of local rainfall and therefore its d-excess (Vuille et al., 2003). Most of the d-excess values of local precipitation are above the global average value of 10 ‰ (Craig, 1961), indicating that most of the water masses were formed in regions with relative humidity higher than 85%. The d-excess variability of rainwater follows the same trend as that of drip water in Río Secreto cave during the three hydrological years, suggesting the transmission of d-excess from rainfall to drip water is happening rapidly. The d-excess variability of rainfall is modulated by drips from station A to a larger extent than those from station LF. Abrupt changes in d-excess are coeval with abrupt changes in drip rates from station B, providing evidence of a rapid response of the system to changes in the amount of precipitation (Supplementary Fig. A.4.). Surprisingly, the d-excess of groundwater and drip water of Fénix shows weekly variability, which indicates that although both reservoirs are likely very large, and therefore maintain a very stable composition of $\delta^{18}O$, both are influenced by moisture source changes. Groundwater and Fénix d-excess variability is modest, however, compared to the other drips and rainfall (Fig. 9).

5.3. Local Meteoric Water Line and the role of evaporation

Fig. 4 shows linear relationships between $\delta^{18}O$ and δD of local rainfall (i.e. local meteoric water line, LMWL) and of drip waters (i.e. drip water line DWL). The observed

LMWL (slope = 8.17‰, 95% confidence interval, CI = 7.7–8.6‰) is very close to the global meteoric water line (GMWL, slope = 8‰) (Craig, 1961; Rozanski et al., 1993). The slope of the DWL, however, is lower and statistically distinct (slope = 7.40‰, CI 95% = 7.3–7.5‰) from the LMWL. We propose that the lower slope of the DWL relative to the LMWL does not reflect evaporation of drip water, but that drip waters preferentially incorporate summer/rainy season precipitation (June-Nov), which makes up 80% of total annual rainfall. A LMWL including only the rainy season (slope = 7.6 ‰, CI 95% = 6.7–8.5‰) is statistically indistinguishable from the DWL (7.4‰), supporting this inference (Supplementary Table A.2). Furthermore, linear relationships between $\delta^{18}O$ and δD of 12 out of 15 drip sites have slopes statistically similar to that of the rainy season LMWL (Table A.2). Exceptions were Aquiles, A3 and Fénix, probably due to their different water residence times and integration periods relative to rainfall variability (See Supplementary Table A.2). Fénix has a very shallow slope since the composition of $\delta^{18}O$ is practically constant, and its values are located above the GMWL. There are several lines of evidence that suggest evaporative processes did not control the isotopic composition of drip water: (i) drip water isotopic values are similar to the LMWL; (ii) a drip water isotopic composition is similar to that of coeval rainfall; (iii) drip water mean annual $\delta^{18}O$ compositions from stations A and B closely resemble the annual amount-weighted $\delta^{18}O$ composition of rainfall; (iv) drip water average $\delta^{18}O$ composition from Fénix is 1-2‰ more negative than the annual amount-weighted $\delta^{18}O$ composition of rainfall, and; (v) cave air relative humidity was at or near 100% during the entire recorded period.

5.4. Groundwater

As previously mentioned, the isotopic composition of groundwater is consistent with the annual amount-weighted isotopic composition of rainfall. The temporal isotopic stability of groundwater in the Río Secreto system over the three hydrologic years studied suggests that it integrates several years of rainfall. It is well known that groundwater integrates long-term rainfall events (e.g. 5–10 years) which is reflected in its isotopic composition (Clark and Fritz, 1997; Wassenaar et al., 2009).

5.5. Effective recharge

In regions of little surface runoff, such as the YP, the conventional approach to estimate an effective recharge has been to use precipitation (P) minus evapotranspiration (E) (Gondwe et al. 2010, Bauer-Gottwein et al., 2011). Based on this approach, instrumental weather data suggests that effective recharge in most of the YP would occur from only June to November, and that some locales would experience no recharge throughout the year (Lases-Hernández, 2013). Playa del Carmen in particular would experience effective recharge only during the months of June, September, October and November, representing ~16% of total annual rainfall (Supplementary Table A.4). This result is consistent with independent estimates of effective recharge in the YP based on P-E (15–17% of total annual precipitation) (Gondwe et al., 2010, Bauer-Gottwein et al., 2011).

This conventional approach to estimate effective recharge, however, does not take into consideration the permeability of the local karst. In the case of the YP, where regional permeability is high and varies significantly (Bauer-Gottwein et al., 2011), these estimates are expected to underestimate recharge, as suggested by independent approaches (Thomas, 1999; Beddows, 2004). Our study provides compelling evidence that the true recharge in the Río Secreto Cave system closely reflects precipitation amount and not P-E. This inference is supported by: (i) annual drip water $\delta^{18}O$ composition similar to the annual amount-weighted $\delta^{18}O$ composition of rainfall at stations A and B (Fig. 5); (ii) annual $\delta^{18}O$ values of drip waters at station LF, which show a strong flow response to individual precipitation events, almost identical to the annual mean $\delta^{18}O$ composition of rainfall (unweighted) over three consecutive years (Fig. 5); (iii) drip water stable isotopic variability in all stations following that of rainfall throughout the year, even during months where P-E is negative (Supplementary Table A.4), and; (iv) drip rate variability at all stations responding to rainfall amount variability throughout the year. This inference is in agreement with previous studies that determined the effective recharge in the northeastern YP based on field measurements, which also suggest that the conventional approach to estimate effective recharge (i.e. P-E) underestimates the true recharge (Thomas, 1999; Beddows, 2004). The expectation *a priori* that effective recharge simply reflects the precipitation to evapotranspiration balance is, therefore, unrealistic in some karstic regions with high permeability, e.g., the northeastern YP.

5.6. Paleoclimate implications

Our results have implications for paleo-rainfall reconstruction from stalagmite $\delta^{18}O$ records, which offer a unique opportunity to reconstruct the history of precipitation, monsoon intensity and tropical cyclone activity going back thousands of years. (Burns, 2004; Frappier et al., 2007b; Medina-Elizalde et al., 2010; Wang et al., 2001, 2007). Rarely, however, have these studies included information on how the rainfall isotopic signal is transferred to cave drip water, which are the values ultimately recorded in speleothems. This information is important in assessing how much time is integrated into the drip water isotopic signal for a given stalagmite. The results from this study suggest that individual drip waters can represent a range of integration of the isotopic composition of rainfall, and therefore, of rainfall accumulation. In addition, this study shows that significant variability among drips may be observed when sampling locations are only few meters apart.

We observe two basic time-integration modes of rainfall as reflected by the isotopic composition of drip waters. In one, drip waters isotopic values closely record individual rainfall events albeit with a slight amplitude modulation. In the second, drip waters isotopic values represent an

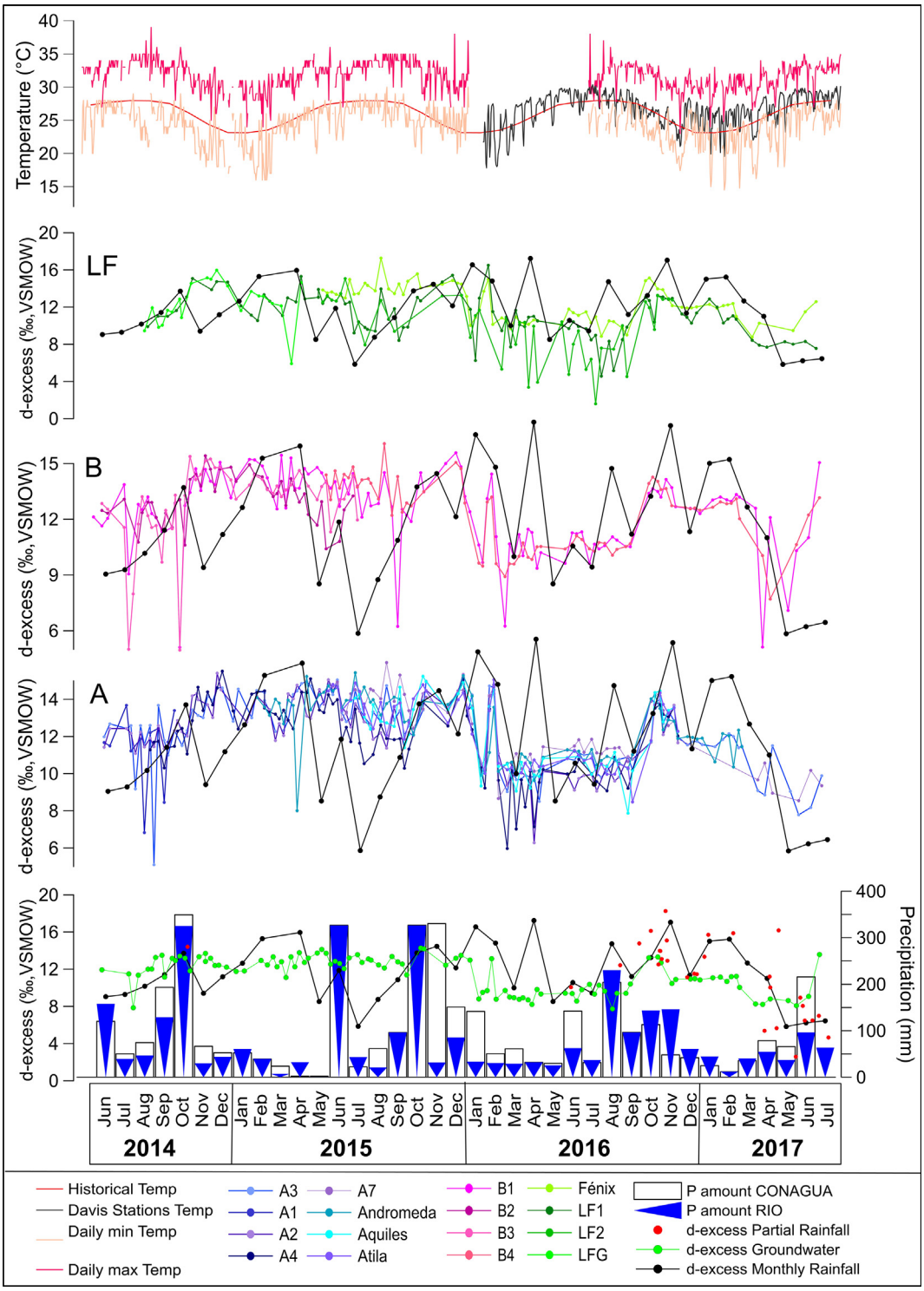

Fig. 9. Upper Panel shows the minimum, maximum, average and historical temperatures of Playa del Carmen. LF, B and A panels show the d-excess data from rainfall and drip waters at each of these stations. Lower Panel shows precipitation amount collected at Río Secreto cave and by CONAGUA in Cancún, Playa del Carmen and Cozumel (See Section 3.1), and the d-excess from rainfall and groundwater.

entire year or more of rainfall accumulation. Additionally, we find that a drip can integrate several years of large precipitation events (e.g. Fénix). In light of this evidence, particular caution needs to be applied when stalagmite $\delta^{18}O$ records are sampled at subannual time scales. At this temporal resolution, stalagmites may represent cumulative rainfall amounts from individual rainfall events (e.g. LF1) or integrate over a year or longer (e.g. A3). Subannual

sampling resolution of a stalagmite almost never provides an accurate representation of the true seasonal cycle of precipitation. Furthermore, out of the 16 drips examined in this study perhaps only two, LF1 and LF2, could be potentially suitable for reconstructing the history of tropical cyclones *sensu* Frappier et al. (2007a). Amplitude reduction of the isotopic signal of short-lived rainfall events is expected in nearly all cases, however, which would greatly lessen the negative isotopic anomalies characteristic of tropical cyclones (Lawrence and Gedzelman, 1996; Lawrence, 1998; Gedzelman et al., 2003; Vieten et al., 2018).

The observation that most drip waters record the amount-weighted $\delta^{18}O$ composition of precipitation when integrated over a year or longer provides support to quantitative reconstructions of annual precipitation variability (Bar-Matthews and Ayalon, 2004; Lachniet et al., 2012, 2017; Medina-Elizalde and Rohling, 2012; Medina-Elizalde et al., 2017). A potential bias in these records could be produced, however, when stalagmite $\delta^{18}O$ values reflect a long-term integration of a summer-biased drip, such as Fénix. Our study suggests that this type of drip, at least in Río Secreto cave, is uncommon. Another potential bias could occur in association with drought years when summer monsoon precipitation fails, as we document in this study for the year 2016. In this case, due to the isotopic inertia of drips fed by relatively large water reservoirs, stalagmite $\delta^{18}O$ could underestimate the magnitude of a drought during year one and would be expected to record the full magnitude of multiyear drought with a delay of at least one year. Finally, because the cave can experience ventilation in some chambers and some drips are seasonal, more detailed studies with farmed calcite should be carried out to assess potential seasonal stalagmite growth biases.

6. CONCLUSIONS

We monitored surface and cave physicochemical conditions, including the $\delta^{18}O$ and δD of over 1200 groundwater, drip water and rainfall samples in the Río Secreto cave system, located in the Yucatán Peninsula, México, for three consecutive years. Isotopic data from drip water is interpreted to reflect two end-members of integration of rainfall amount: approximating the annual amount-weighted isotopic composition of rainfall or the annual arithmetic average isotopic composition (unweighted). Drip waters represent different integration times of rainfall accumulation with a lag from few days to up to three months and can be placed within the context of these two end-members. The intra-annual isotopic amplitude variability of 16 drips examined represents 5% to 95% of the observed isotopic amplitude of rainfall. Drip waters that do not modulate the isotopic amplitude of rainfall and that preserve the isotopic signal of individual rainfall events are, however, rare. Only 2 drips out of 16 were found to have potential to record the negative rainfall isotopic excursions associated with tropical cyclones if sampled at weekly resolution, but these still underrepresent the isotopic magnitude of individual rainfall events. Because the isotopic composition of drip waters approximate either the annual arithmetic average of rainfall (small reservoir effect) or the annual amount-weighted isotopic composition of rainfall (larger reservoir effect) when integrated over a year, quantitative rainfall reconstructions from stalagmite $\delta^{18}O$ records are feasible on annual or longer resolutions (e.g. *sensu* Medina-Elizalde and Rohling, 2012). Stalagmite $\delta^{18}O$ sub-annual variability, however, is likely to underestimate the seasonal variability of rainfall amount due to amplitude modulation of the rainfall isotopic signal during infiltration into the cave environment. We found that an individual drip may record the most intense rainfall events that occur during the summer season or, alternatively, may integrate over three years of rainfall accumulation. Isotopic inertia associated with most drip waters results in an underestimation of the magnitude of a drought that lasts one year, and a delay of at least one year in recording multiyear droughts by stalagmite $\delta^{18}O$ records. Lastly, we provide evidence that the effective recharge in the YP karst system is not limited to the months when precipitation exceeds evaporation. This important hydrological finding has implications for freshwater management and adaptation strategies to climate change in the YP.

ACKNOWLEDGEMENTS

We appreciate the enthusiastic family of Río Secreto Nature Reserve for their incredible support during the last four years of cave fieldwork. We specially thank Tania Ramírez, Otto Von Bertrab, Rodrigo Pimienta, Raúl Padilla, Alan Borjas, Isabel Barradas, Mely Ramos, Dan Venegas, Mónica Fernández, Natalia Dixon, Lu Faccioli, Nunes Joao and Alfredo Ponce. We thank Julio León for the digitalization of Fig. 5.We also thank Peter Sprouse for providing Río Secreto Cave Map. We appreciate the revisions to this article by Dr. Jay Quade, Dr. Patricia Beddows, Dr. Juan Pablo Bernal Uruchurtu and four anonymous reviewers that helped to increase the solidity and clarity of this paper. We thank CONACYT-Mexico for providing a scholarship to support Fernanda Lases-Hernandez PhD studies at UNAM (Grant No. 440572). This project was funded by NSF Grant #1502836 and Waitt Grant #W457-16.

APPENDIX A. SUPPLEMENTARY MATERIAL

Supplementary data to this article can be found online at https://doi.org/10.1016/j.gca.2018.11.028.

REFERENCES

Akers P. D., Brook G. A., Railsback L. B., Liang F., Iannon G., Webster J. W., Reeder P. P., Cheng H. and Edwards R. L. (2016) An extended and higher-resolution record of climate and land use from stalagmite MC01 from Macal Chasm, Belize, revealing connections between major dry events, overall climate variability, and Maya sociopolitical changes. *Palaeogeogr. Palaeoclimatol. Palaeoecol* **459**, 268–288.

Allen R.G., Pereira L.S., Raes D. and Smith M. (1998) In: *United Nations Food and Agriculture Organization, Irrigation and Drainage Paper 56* (eds. R.G. Allen, L.S. Pereira, D.Raes and M.Smith), Crop Evapotranspiration: Guidelines for Computing Crop Water Requirements. Rome, Italy, pp. 300.

Arbel Y., Greenbaum N., Lange J. and Inbar M. (2010) Infiltration processes and flow rates in developed karst vadose zone using tracers in cave drips. *Earth Surf. Process. Landf.* **35**, 1682–1693.

Ayalon A., Bar-Matthews M. and Sass E. (1998) Rainfall-recharge relationships within a karstic terrain in the Eastern Mediterranean semi-arid region, Israel: $\delta^{18}O$ and δD characteristics. *J. Hydrol.* **207**, 18–31.

Bakalowicz M. (2012) Epikarst. In *Encyclopedia of Caves* (ed. D. C. Culver). Academic Press, Amsterdam, pp. 284–288.

Baldini L. M., Baldini J. U. L., McElwaine J., Frappier A. B., Asmerom Y., Liu K. B., Prufer K., Ridley H. E., Polyak V., Kennett D. J., Macpherson C. G., Aquino V. V., Awe J. and Breitenbach S. F. M. (2016) Persistent northward North Atlantic tropical cyclone track migration over the past five centuries. *Sci. Rep.* **6**, 37522.

Baldini J. U., Baldini L. M., McDermott F. and Clipson N. (2006) Carbon dioxide sources, sinks, and spatial variability in shallow temperate zone caves: evidence from Ballynamintra Cave, Ireland. *J. Caves Karst Stud.* **68**, 4–11.

Bar-Matthews M. and Ayalon A. (2004) Speleothems as paleoclimate indicators, a case study from Soreq cave located in the Eastern Mediterranean region, Israel. In *Past Climate Variability through Europe and Africa* (eds. R. W. Battarbee, F. Gasse and C. E. Stickley). Kluer Academic Publishers Dordrecht, The Netherlands, pp. 343–362.

Bauer-Gottwein P., Gondwe B. R., Charvet G., Marín L. E., Rebolledo-Vieyra M. and Merediz-Alonso G. (2011) the Yucatan Peninsula karst aquifer, Mexico. *Hydrogeol. J.* **19**, 507–524.

Bautista F., Palacio-Aponte G., Quintana P. and Zinck J. A. (2011) Spatial distribution and development of soils in tropical karst areas from the Peninsula of Yucatan, Mexico. *Geomorphology* **135**, 308–321.

Beddows P.A. (2004) Groundwater hydrology of a coastal conduit carbonate aquifer: Caribbean coast of the Yucatán Peninsula, México. PhD thesis, Sch. of Geogr. Sci. Univ. of Bristol, UK.

Beddows P. A. and Mallon E. K. (2018) Cave pearl data logger: a flexible arduino-based logging platform for long-term monitoring in harsh environments. *Sensors* **18**, 530.

Beddows P. A., Mandić M., Ford D. C. and Schwarcz H. P. (2016) Oxygen and hydrogen isotopic variations between adjacent drips in three caves at increasing elevation in a temperate coastal rainforest, Vancouver Island, Canada. *Geochim. Cosmochim. Acta* **172**, 370–386.

Bradley C., Baker A., Jex C. N. and Leng M. J. (2010) Hydrological uncertainties in the modelling of cave drip-water $\delta^{18}O$ and the implications for stalagmite palaeoclimate reconstructions. *Quat. Sci. Rev.* **29**, 2201–2214.

Burns S. J. (2004) Indian Ocean climate and an absolute chronology over Dansgaard/Oeschger events 9 to 13. *Science* **305**, 1567-1567.

Cabadas-Báez H., Solleiro-Rebolledo E., Sedov S., Pi-Puig T. and Gama-Castro J. (2010) Pedosediments of karstic sinkholes in the eolianites of NE Yucatán: a record of Late Quaternary soil development, geomorphic processes and landscape stability. *Geomorphology* **122**, 323–337.

Cheng H., Edwards R. L., Sinha A., Spötl C., Yi L., Chen S., Kelly M., Kathayat G., Wang X., Li X., Kong X., Wang Y., Ning Y. and Zhang H. (2016) The Asian monsoon over the past 640,000 years and ice age terminations. *Nature* **534**, 640–646.

Clark I. D. and Fritz P. (1997) *Environmental Isotopes in Hydrogeology*. CRC/Lewis, New York, p. 328, ISBN: 9781566702492.

Cobb K. M., Adkins J. F., Partin J. W. and Clark B. (2007) Regional-scale climate influences on temporal variations of rainwater and cave dripwater oxygen isotopes in northern Borneo. *Earth Planet. Sci. Lett.* **263**, 207–220.

CONAGUA. (2017) Comisión Nacional del Agua. Servicio Meteorológico Nacional, México. Available at <http://smn.cna.gob.mx/>. Data obtained in 2017.

Cowan B. D., Osborne M. C. and Banner J. L. (2013) Temporal variability of cave-air CO_2 in central Texas. *J Cave Karst Stud.* **75**, 38.

Craig H. (1961) Isotopic variations in meteoric waters. *Science* **133**, 1702–1703.

Cuthbert M. O., Baker A., Jex C. N., Graham P. W., Treble P., Andersen M. S. and Acworth R. I. (2014) Drip water isotopes in semi-arid karst: implications for speleothem paleoclimatology. *Earth Planet. Sci. Lett.* **395**, 194–204.

Cruz F. (2005) Stable isotope study of cave percolation waters in subtropical Brazil: implications for paleoclimate inferences from speleothems. *Chem. Geol.* **220**, 245–262.

Czuppon G., Demény A., Leél-Őssy S., Óvari M., Molnár M., Stieber J., Kiss K., Kármán K., Surányi G. and Haszpra L. (2018) Cave monitoring in the Béke and Baradla caves. (Northeastern Hungary): implications for the conditions for the formation cave carbonates. *Int. J. Speleol.* **47**, 13–28.

Dansgaard W. (1964) Stable isotopes in precipitation. *Tellus* **16**, 436–468.

Duan W., Ruan J., Luo W., Li T., Tian L., Zeng G., Zhang D., Bai Y., Li J., Tao T., Zhang P., Baker A. and Tan M. (2016) The transfer of seasonal isotopic variability between precipitation and drip water at eight caves in the monsoon regions of China. *Geochim. Cosmochim. Acta* **183**, 250–266.

Fairchild I. and Baker A. (2012) *Speleothem Science*. Wiley-Blackwell.

Fairchild I. J., Tuckwell G. W., Baker A. and Tooth A. F. (2006) Modelling of dripwater hydrology and hydrogeochemistry in a weakly karstified aquifer (Bath, UK): implications for climate change studies. *J. Hydrol.* **321**, 213–231.

Frappier A., Knutson T., Liu K. B. and Emanuel K. (2007a) Perspective: coordinating paleoclimate research on tropical cyclones with hurricane-climate theory and modelling. *Tellus* **59**, 529–537.

Frappier A. B., Sahagian D., Carpenter S. J., González L. A. and Frappier B. R. (2007b) Stalagmite stable isotope record of recent tropical cyclone events. *Geology* **35**, 111–114.

Frisia S., Fairchild I. J., Fohlmeister J., Miorandi R., Spöt C. and Borsato A. (2011) Carbon mass-balance modelling and carbon isotope exchange processes in dynamic caves. *Geochim. Cosmochim. Acta* **75**, 380–400.

Fuller L., Baker A., Fairchild I. J., Spötl C., Marca-Bell A., Rowe P. and Dennis P. F. (2008) Isotope hydrology of dripwaters in a Scottish cave and implications for stalagmite palaeoclimate research. *Hydrol. Earth Syst. Sci.* **12**, 1065–1074.

Genty D. (2008) Palaeoclimate research in Villars Cave (Dordogne, SW-France). *Int. J. Speleol.* **37**, 173–191.

Genty D., Labuhn I., Hoffmann G., Danis P. A., Mestre O., Bourges F., Wainer K., Massault M., Van Exter S., Rágnier E., Orengo P., Falourd S. and Minster B. (2014) Rainfall and cave water isotopic relationships in two South-France sites. *Geochim. Cosmochim. Acta* **131**, 323–343.

Gedzelman S., Hindman E. and Zhang X. (2003) Probing hurricanes with stable isotopes of rain and water vapor. *Mon. Wea. Rev.* **131**, 1112–1127.

Gondwe B. R., Lerer S., Stisen S., Marín L., Rebolledo-Vieyra M., Merediz-Alonso G. and Bauer-Gottwein P. (2010) Hydrogeology of the south-eastern Yucatan Peninsula: new insights from water level measurements, geochemistry, geophysics and remote sensing. *J. Hydrol.* **389**, 1–17.

Hartmann A. and Baker A. (2017) Modelling karst vadose zone hydrology and its relevance for paleoclimate reconstruction. *Earth-Sci. Rev.* **172**, 178–192.

IAEA (2014) IAEA/GNIP precipitation sampling guide. Available at <http://www-naweb.iaea.org>

Karmalkar A. V., Bradley R. S. and Diaz H. F. (2011) Climate change in Central America and Mexico: regional climate model validation and climate change projections. *Clim. Dyn.* **37**(3–4), 605.

Kennett D. J., Breitenbach S. F., Aquino V. V., Asmerom Y., Awe J., Baldini J. U., Bartlein P., Culleton B. J., Ebert C. and Jazwa C. (2012) Development and disintegration of Maya political systems in response to climate change. *Science* **338**, 788–791.

Lachniet M. S. and Patterson W. P. (2009) Oxygen isotope values of precipitation and surface waters in northern Central America (Belize and Guatemala) are dominated by temperature and amount effects. *Earth Planet. Sci. Lett.* **284**, 435–446.

Lachniet M. S., Bernal J. P., Asmerom Y., Polyak V. and Piperno D. (2012) A 2400-yr Mesoamerican rainfall history links climate and cultural change in Mexico. *Geology* **40**, 259–326.

Lachniet M. S., Asmerom Y., Polyak V. and Bernal J. P. (2017) Two millennia of Mesoamerican monsoon variability driven by Pacific and Atlantic synergistic forcing. *Quat. Sci. Rev.* **155**, 100–113.

Lases-Hernández F. (2013) Análisis Temporal y Espacial de la Influencia de los Ciclones Tropicales en la Precipitación de la Península de Yucatán. Master Thesis, Centro de Investigación Científica de Yucatán, México.

Lawrence J. R. (1998) Isotope spikes from tropical cyclones in surface waters: opportunities in hydrology and paleoclimatology. *Chem. Geol.* **144**, 153–160.

Lawrence J. R. and Gedzelman S. D. (1996) Low stable isotope ratios of tropical cyclone rains. *Geophys. Res. Lett.* **23**, 527–530.

Li B., Yuan D., Qin J., Lin Y. and Zhang M. (2000) Oxygen and carbon isotopic characteristics of rainwater, drip water and present speleothems in a cave in Guilin area, and their environmental meanings. *Sci. China Ser. D-Earth Sci.* **43**, 277–285.

López-Ramos E. (1975) Geological summary of the Yucatan Peninsula. In *The Ocean Basins and Margins, The Gulf of Mexico and the Caribbean* (eds. A. E. M. Nairn and F. G. Stehli). Plenum Press, NY, USA, pp. 257–282.

Luo W., Wang S., Zeng G., Zhu X. and Liu W. (2014) Daily response of drip water isotopes to precipitation in Liangfeng Cave, Guizhou Province, SW China. *Quat. Int.* **349**, 153–158.

Magaña V., Amador J. A. and Medina S. (1999) The midsummer drought over Mexico and Central America. *J. Climate.* **12**, 1577–1588.

McDermott F. (2004) Palaeo-climate reconstruction from stable isotope variations in speleothems: a review. *Quat. Sci. Rev.* **23**, 901–918.

McMonigal K. and Beddows P.(2014) Calcite rafts - rapid deposition of transgressive infill cave sequences as a new paleo sea level proxy. In 2014 GSA Annual Meeting in Vancouver, British Columbia (19–22 October 2014). Vancouver, BC. Canada. # 43-2 (abstr.).

Medina-Elizalde M. and Rohling E. J. (2012) Collapse of Classic Maya civilization related to modest reduction in precipitation. *Science* **335**, 956–959.

Medina-Elizalde M., Burns S. J., Lea D. W., Asmerom Y., von Gunten L., Polyak V., Vuille M. and Karmalkar A. (2010) High resolution stalagmite climate record from the Yucatán Peninsula spanning the Maya terminal classic period. *Earth Planet. Sci. Lett.* **298**, 255–262.

Medina-Elizalde M., Burns S. J., Polanco-Martinez J., Lases-Hernández F., Bradley R., Wang H.-C. and Shen C.-C. (2017) Synchronous precipitation reduction in the American Tropics associated with Heinrich 2. *Sci. Rep.* **7**, 11216.

Medina-Elizalde M., Burns S. J., Polanco-Martínez J. M., Beach T., Lases-Hernández F., Shen C.-C. and Wang H.-C. (2016a) High-resolution speleothem record of precipitation from the Yucatan Peninsula spanning the Maya Preclassic Period. *Glob. Planet. Change.* **138**, 93–102.

Medina-Elizalde M., Polanco-Martínez J. M., Lases-Hernández F., Bradley R. and Burns S. (2016b) Testing the ''tropical storm'' hypothesis of Yucatan Peninsula climate variability during the Maya Terminal Classic Period. *Quat. Res.* **86**, 111–119.

Merlivat L. and Jouzel J. (1979) Global climatic interpretation of the deuterium/oxygen 18 relationship for precipitation. *Jour. Geophys. Res.* **84**, 5029–5033.

Mestas-Nuñez A. M., Enfield D. B. and Zhang C. (2007) Water vapor fluxes over the Intra-Americas Sea: Seasonal and interannual variability and associations with rainfall. *J. Climate.* **20**, 1910–1922.

Muñoz E., Busalacchi A. J., Nigam S. and Ruiz-Barradas A. (2008) Winter and summer structure of the Caribbean low-level jet. *J. Climate.* **21**, 1260–1276.

Oh Y. H. and Kim G. (2011) Factors controlling the air ventilation of a limestone cave revealed by 222 Rn and 220 Rn tracers. *Geosci. J.* **15**, 115–119.

Onac B. P., Pace-Graczyk K. and Atudirei V. (2008) Stable isotope study of precipitation and cave drip water in Florida (USA): implications for speleothem-based paleoclimate studies. *Isot. Environ. Health Sci.* **44**, 149–161.

Orellana R., Espadas C., Conde C. and Gay C. (2009) Atlas. Scenarios Climate Change in the Yucatán Peninsula. In Problemas del desarrollo, (ed. E. Iglesias) Centro de I nvestigación Científica de Yucatán (CICY). Mérida, México 43(168), pp.191–193.

Palaeosens P. M. (2012) Making sense of palaeoclimate sensitivity. *Nature* **491**, 683–691.

Railsback L. B., Liang F., Vidal-Romaní J. R., Garrett K. B., Sellers R. C., Vaqueiro-Rodríguez M., Grandal-d'Anglade A., Cheng H. and Edwards R. L. (2017) Radiometric, isotopic, and petrographic evidence of changing interglacials over the past 550,000 years from six stalagmites from the Serra do Courel in the Cordillera Cantábrica of northwestern Spain. *Palaeogeogr. Palaeoclimatol. Palaeoecol.* **466**, 137–152.

Rau G. C., Cuthbert M. O., Andersen M. S., Baker A., Rutlidge H., Markowska M., Roshan H., Marjo C. E., Graham P. W. and Acworth R. I. (2015) Controls on cave drip water temperature and implications for speleothem-based paleoclimate reconstructions. *Quat. Sci. Rev.* **127**, 19–36.

Riechelmann D. F. C., Schröder-Ritzrau A., Scholz D., Fohlmeister J., Spötl C., Richter D. K. and Mangini A. (2011) Monitoring Bunker Cave (NW Germany): a prerequisite to interpret geochemical proxy data of speleothems from this site. *J. Hydrol.* **409**, 682–695.

Riechelmann S., Schröder-Ritzrau A., Spötl C., Riechelmann D. F. C., Richter D. K., Mangini A., Frank N., Breitenbach S. F. M. and Immenhauser A. (2017) Sensitivity of Bunker Cave to climatic forcings highlighted through multi-annual monitoring of rain-, soil-, and dripwaters. *Chem. Geol.* **449**, 194–205.

Rozanski K., Araguas-Araguas L. and Gonfiantini R. (1993) Isotopic patterns in modern global precipitation. In *Climate Change in Continental Isotope Records*, vol. 78 (eds. P. K. Swart, K. C. Lohman, J. McKenzie and S. Savin). American Geophysical Union Monograph, pp. 1–36.

Smart P. L. and Friederich H. (1987) Water movement and storage in the unsaturated zone of a maturely karstified aquifer, Mendip Hills, England. In *Proceedings of the Conference on Environmental Problems in Karst Terrains and their Solutions*. National Water Well Association, Dublin Ohio, pp. 59–87.

Smerdon J. E., Pollack H. N., Enz J. W. and Lewis M. J. (2003) Conduction-dominated heat transport of the annual temperature signal in soil. *J. Geophys. Res.: Solid Earth* **108**.

Sprouse P,. Stan A., Ediger G., Graham K., Lloyd C., Moore D., Rincón J. (cartoonists). Addison A., Bordignon M., Bryant M., Burgos J., Cahun H., Alanis A., Ediger G., Ferreira A., Gouila C., Munguía M., Ramírez T., Rojo R., Solignac G., Sprouse P., Sprouse T, Vela G., Vela J., Von Bertrab O., Yañez G., Zabaleta M., Zappitello M., Zappitello S. and others (topographers) (2017) Map of the Pool Tunich System. Playa del Carmen, Quintana Roo, Mexico. Contact <Peter@zaraenvironmental.com>.

Thomas C. (1999) Aspects hydrogéologiques du Yucatan (Mexique). *Karstologia* **34**, 9–22.

Vieten R., Warken S., Winter A., Schröder-Ritzrau A., Scholz D. and Spötl C. (2018) Hurricane impact on seepage water in Larga Cave, Puerto Rico. *J. Geophys. Res. Biogeosci.* **123**, 879–888.

Vieten R., Winter A., Warken S. F., Schröder-Ritzrau A., Miller T. E. and Scholz D. (2016) Seasonal temperature variations controlling cave ventilation processes in Cueva Larga, Puerto Rico. *Int. J. Speleol.* **45**, 7.

Vuille M., Bradley R. S., Healy R., Werner M., Hardy D. R., Thompson L. G. and Keimig F. (2003) Modeling $\delta^{18}O$ in precipitation over the tropical Americas: 2. Simulation of the stable isotope signal in Andean ice cores. *J. Geophys. Res.* **108**, 4175.

Wang X., Auler A. S., Edwards R. L., Cheng H., Ito E., Wang Y., Kong X. and Solheid M. (2007) Millennial-scale precipitation changes in southern Brazil over the past 90,000 years. *Geophys. Res. Lett.* **34**, L23701.

Wang Y. J., Cheng H., Edwards R. L., An Z. S., Wu J. Y., Shen C. C. and Dorale J. A. (2001) A high-resolution absolute-dated Late Pleistocene monsoon record from Hulu Cave, China. *Science* **294**, 2345–2348.

Ward W. C. (1985) Quaternary geology of northeastern Yucatan Peninsula. In *Geology and Hydrogeology of the Yucatan and Quaternary Geology of Northeastern Yucatan Peninsula* (eds. A. E. Weidie, W. C. Ward and W. Back). New Orleans Geological Society, New Orleans, LA, pp. 23–95.

Wassenaar L. I., Van Wilgenburg S. L., Larson K. and Hobson K. A. (2009) A groundwater isoscape (δD, $\delta^{18}O$) for Mexico. *J. Geochem. Explor.* **102**, 123–136.

Williams P. P. W. and Fowler A. (2002) Relationship between oxygen isotopes in rainfall, cave percolation waters and speleothem calcite at Waitomo, New Zealand. *J. Hydrol. New. Zeal.* **41**, 53–70.

Wigley T. M. L. and Brown M. C. (1976) The physics of caves. In *The Science of Speleology* (eds. T. D. Ford and C. H. D. Cullingford). Academic Press, London, pp. 329–358.

Worthington S. R. H. and Ford D. C. (2009) Self-organized permeability in carbonate aquifers. *Ground Water* **47**, 326–336.

Yonge C., Ford D., Gray J. and Schwarcz H. (1985) Stable isotope studies of cave seepage water. *Chem. Geol.* **58**, 97–105.

Associate editor: Jay Quade